25 Mar 2024

Nitrene-Transfer Chemistry To C-H And C=C Bonds Mediated By Triangular Coinage Metal Platforms Supported By Triply Bridging Pnictogen Elements Sb(III) And Bi(III)

Meenakshi Sharma

Reece M. Fritz

Joseph O. Adebanjo

Zhou Lu

et. al. For a complete list of authors, see https://scholarsmine.mst.edu/chem_facwork/3685

Recommended Citation

M. Sharma et al., "Nitrene-Transfer Chemistry To C-H And C=C Bonds Mediated By Triangular Coinage Metal Platforms Supported By Triply Bridging Pnictogen Elements Sb(III) And Bi(III)," *Organometallics*, vol. 43, no. 6, pp. 634 - 652, American Chemical Society, Mar 2024.
The definitive version is available at https://doi.org/10.1021/acs.organomet.3c00493

ORGANOMETALLICS

pubs.acs.org/Organometallics Article

Nitrene-Transfer Chemistry to C−H and C═C Bonds Mediated by Triangular Coinage Metal Platforms Supported by Triply Bridging Pnictogen Elements Sb(III) and Bi(III)

Meenakshi Sharma, Reece M. Fritz, Joseph O. Adebanjo, Zhou Lu, Thomas R. Cundari, Mohammad A. Omary, Amitava Choudhury, and Pericles Stavropoulos*

Cite This: *Organometallics* 2024, 43, 634−652 Read Online

ACCESS | Metrics & More | Article Recommendations | Supporting Information

ABSTRACT: Tripodal ligands (TMG_3trphen-E) that feature heavy pnictogen elements (E = Sb(III), Bi(III)) and tetramethylguanidinyl (TMG) arms have been explored in stabilizing Cu(I) and Ag(I) sites and facilitating nitrene-transfer chemistry. Compounds $[(TMG_3trphen\text{-}E)M_3(\mu\text{-}X)_3]$ (M = Cu(I), Ag(I); X = Cl, Br, I) have been generated upon extraction of $M_3(\mu\text{-}X)_3$ units from MX sources, exhibiting support of the crown-shaped $M_3(\mu\text{-}X)_3$ fragment by $M\text{−}N_{TMG}$ bonds and triply bridging E → M_3 interactions. Orbital interactions between Cu(I) sites and N_{TMG} residues are more dominant than Sb/Bi → Cu_3 donor interactions between the Sb 5s or Bi 6s orbitals and admixed Cu 4s/3d orbitals, with larger interaction energies computed for Sb → Cu_3. Nonhalogenated copper compounds $[(TMG_3trphen\text{-}E)_2Cu_2]^{2+}2Y^-$ (Y = PF_6, $B(C_6F_5)_4$) have been synthesized via dechlorination by $TlPF_6$ or by application of halide-free Cu(I) sources with TMG_3trphen-E ligands. Nitrene-transfer to olefins mediated by $[(TMG_3trphen\text{-}E)Cu_3(\mu\text{-}Cl)_3]$ (E = Sb and Bi) affords aziridines in good yields, primarily for unencumbered styrenes and with the more robust Sb catalyst. Amination of C−H bonds is most effective with sec-benzylic substrates and requires a more electrophilic nitrene (NTces) to achieve practicable yields with halogenated or nonhalogenated copper precursors. Hammett plots indicate that the competitive amination of para-substituted ethylbenzenes enabled by $[(TMG_3trphen\text{-}Sb)Cu_3(\mu\text{-}Cl)_3]$ involves stepwise C−H functionalization.

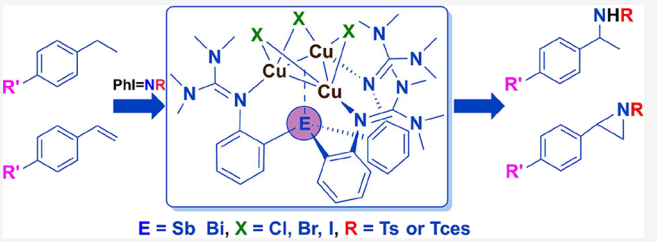

INTRODUCTION

The development of C−N bond construction methodologies encompasses various pathways directed toward inserting nitrogen functionalities into carbonaceous feedstock for the synthesis of a diverse body of commodity and high-value chemicals (pharmaceuticals, agrochemicals, polymers, semiconductors, catalysts, solvents, and household chemicals).[1] Among different approaches, the insertion of nitrenes (NR) or nitrenoids (NR(X)) into C−H bonds or their addition to C═C bonds affords valuable products of amination and aziridination, respectively, as well as derivatives (such as amidines or five-membered *N*-heterocycles) in the presence of additional substrates (usually unsaturated entities).[2] This direct functionalization of C−H/C═C feedstock belongs to the general category of atom/group-transfer chemistry,[3] pertaining to a wide variety of common atoms (e.g., H/D, N, O, S, and halogen) or groups (e.g., BR_2, CR_2/CR_3, NR/NR_2, and N_3).[4−12] Biological atom/group-transfer analogs have frequently provided inspiration and opportunities for further development via biomimetic approaches and enzyme engineering.[13] The direct C−H/C═C functionalization obviates the need for constructing energetic C−X precursors (X = leaving or directing group) but raises challenges for achieving acceptable levels of reactivity and selectivity.[14] Taking C−N bond construction from C−H/C═C feedstock as an example, both metal-free[15] and metal-dependent catalytic systems[2,16] have been advanced to overcome these challenges. Notwithstanding the expense and toxicity involved, platinum-group metal catalysts have been frequently invoked,[17] but nonprecious, first-row transition metal reagents[18] have found increasing use. The latter usually raise the possibility of single-electron steps that provide avenues to radical pathways, which may thus offer intriguing alternatives to closed-shell two-electron processes.

In recent work, in our laboratory, we have developed a family of divalent base metals (Mn, Fe, Co, and Ni) and monovalent coinage metal catalysts (Cu and Ag), supported by tripodal trisamido/imino-amine and bipodal bisamido/imino-amine ligands (Chart 1).[19] The weak ligand field and the ability to decorate the equatorial amido/imino residues by a

Received: November 29, 2023
Revised: February 25, 2024
Accepted: February 26, 2024
Published: March 11, 2024

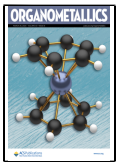

https://doi.org/10.1021/acs.organomet.3c00493
Organometallics 2024, 43, 634−652

Chart 1. Previously Explored Reagents Supported by Axial N_{amine} Coordination

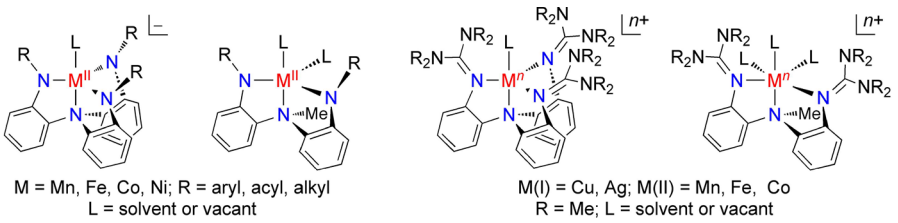

Scheme 1. Synthesis of Ligands Employed in this Study

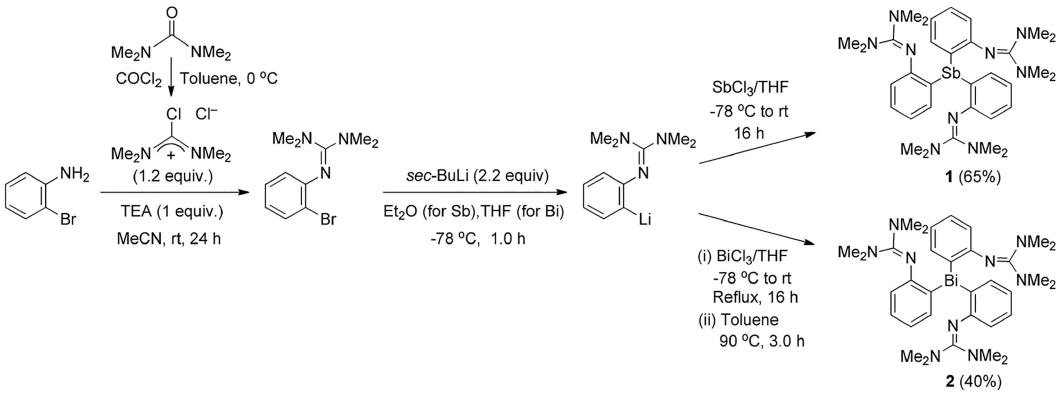

Scheme 2. Synthesis of Metal Halide Compounds

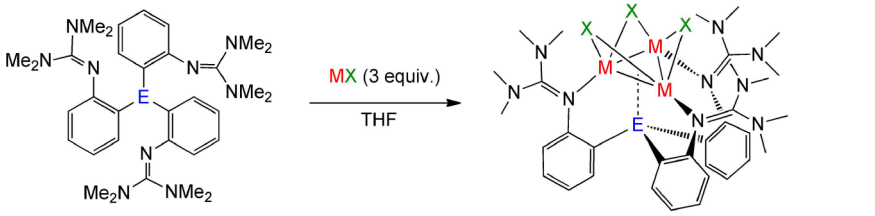

wide range of aryl, acyl, alkyl, and guanidinyl arms has given rise to a plethora of anionic, neutral, and cationic catalysts employed in nitrene transfer to C−H and C=C bonds of hydrocarbons. These tripodal and bipodal ligand scaffolds are analogs of the iconic $N(CH_2CH_2NH_2)_3$ (TREN) and bipodal $N(CH_2CH_2NH_2)_2Me$ frameworks[20−22] but rely on phenylene rather than ethylene linkers, resulting in metal reagents that tend to be more reactive in atom/group-transfer chemistry. Versions of the anionic tripodal metal compounds have also been nicely explored in bimetallic synthesis and catalysis.[23] In general, anionic versions tend to be more appropriate for aziridination reactions,[24] whereas the much more reactive cationic analogs, especially those decorated with tetramethylated guanidinyl arms (extensively studied in TREN chemistry),[25,26] can be effectively employed both in C−H aminations/amidinations (Cu reagents)[27] and C=C aziridinations, in tandem with five-membered *N*-heterocycle synthesis (Mn, Fe, or Co reagents).[28]

In all cases noted above, the axial coordination site is occupied by an N_{amine} atom. With the present work, we are launching an effort toward replacing the apical N_{amine} residue with more weakly electron-donating and potentially electron-accepting Sb(III) and Bi(III) residues.[29] It is anticipated[30] that electron-deficient apical elements can enhance the electrophilicity of any axially positioned metal-nitrene moiety and, therefore, increase reactivity for challenging C−H substrates. Of course, the pnictogen elements generate significantly more sizable ligand cavities than those examined with the tripodal $[N_3N_{amine}]$ scaffolds noted above. Hence, in this publication, we aspire to explore the geometric and electronic characteristics of metal reagents that can be accessed with these axial Sb/Bi containing ligands and provide an initial account of their nitrene-transfer reactivity. We chose to first explore Cu(I) and to a lesser extent Ag(I) sites in tandem with equatorial tetramethylguanidinyl (TMG) residues, given our successful application of the analogous $[(N_3N_{amine})Cu^I]^+$ reagent in the past.[27]

RESULTS AND DISCUSSION

Synthesis of Ligands. The tripodal ligands TMG_3trphen-Sb (**1**) and TMG_3trphen-Bi (**2**) used in this study are synthesized by a concise method (Scheme 1). First, the trimethylguanidinyl groups (TMG) are installed by coupling 2-bromoaniline and chlorotetramethylformamidinium chloride (prepared from tetramethylurea and oxalyl chloride) in the presence of triethylamine in acetonitrile, followed by low-temperature lithiation with *sec*-BuLi (or *tert*-BuLi) in diethyl ether (Sb) or tetrahydrofuran (Bi). The electrophiles $SbCl_3$ and $BiCl_3$ are then used in THF (0.33 equiv versus the lithiated product) to install the axial Sb(III) and Bi(III)

https://doi.org/10.1021/acs.organomet.3c00493
Organometallics 2024, 43, 634−652

Scheme 3. Synthesis of Halide-free Metal Compounds

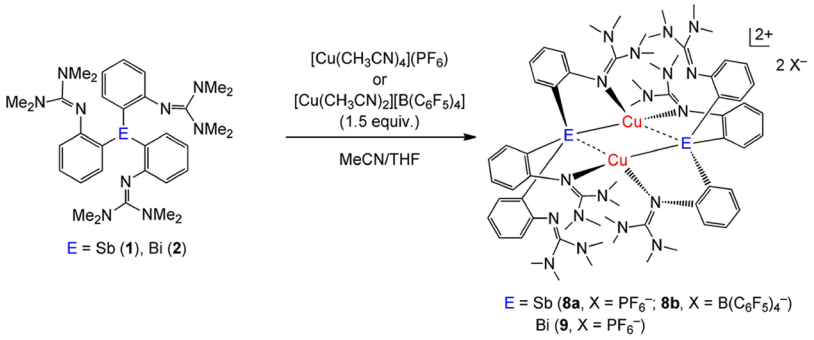

elements, respectively. Both ligands can be crystallized from dichloromethane to provide pure products as white solids in moderate to good yields. The lower yields observed for **2** reflect the thermal instability of the Bi−C bond. ^{1}H NMR spectra (in CD_3CN) indicate that all aryl and methyl groups (NMe_2; sharp single peak at δ = 2.57 (**1**), 2.58 (**2**)) are equivalent at 298 K, hence no significant rotational restrictions are observed at room temperature.

Synthesis of Metal Halide Compounds. The reaction of ligand **1** with 3 equiv of anhydrous CuCl of high purity (beads, ≥99.99%) in THF provides a white solid, which can be dissolved in dichloromethane and obtained as colorless crystals of $[(TMG_3trphen\text{-}Sb)Cu_3(\mu\text{-}Cl)_3]\bullet 4CH_2Cl_2$ (**3**) from concentrated solutions (Scheme 2). The analogous reaction of ligand **2** with CuCl in THF affords the corresponding $[(TMG_3trphen\text{-}Bi)Cu_3(\mu\text{-}Cl)_3]\bullet 4CH_2Cl_2$ (**4**), which can be crystallized from dichloromethane as off-white crystals suitable for X-ray analysis. The corresponding bromo and iodo analogs of **3** can be obtained in a similar manner from the reaction of anhydrous CuX (X = Br, I) with ligand **1** in THF, followed by crystallization from dichloromethane to obtain colorless crystals of $[(TMG_3trphen\text{-}Sb)Cu_3(\mu\text{-}Br)_3]\bullet 4CH_2Cl_2$ (**5**) and $[(TMG_3trphen\text{-}Sb)Cu_3(\mu\text{-}I)_3]\bullet 3CH_2Cl_2$ (**6**), respectively.

A similar trinuclear $Ag_3(\mu\text{-}Cl)_3$ cluster can also be extracted by ligand **1** from anhydrous AgCl (beads, 99.998%) upon prolonged extraction times and crystallized from CH_2Cl_2 as off-white crystals of $[(TMG_3trphen\text{-}Sb)Ag_3(\mu\text{-}Cl)_3]\bullet 3CH_2Cl_2$ (**7**). The same reaction with ligand **2** was not productive even after several weeks of extraction at room temperature or upon heating.

Synthesis of Halide-Free Metal Compounds. For comparative purposes, the coordination chemistry of the stibine (**1**) and bismuthine (**2**) ligand was examined with respect to Cu(I) sites in the absence of any halides. The reaction of either **1** or **2** with 1.5 equiv of $[Cu(NCMe)_4](PF_6)$ in THF/MeCN (Scheme 3) affords colorless crystals of $[(TMG_3trphen\text{-}E)_2Cu_2](PF_6)_2\bullet 2$ solv (E = Sb, solv = THF (**8a**); Bi, solv = Et_2O (**9**)), upon crystallization from THF/MeCN (**8a**) or MeCN/Et_2O (**9**). The Bi compound is only obtained in very low yields, most likely because of the thermal instability of the ligand, as noted above. Incidentally, the corresponding 1:1 ligand/Cu reaction affords intractable mixtures. On one occasion, a few crystals with stoichiometry $[(TMG_3trphen\text{-}Sb)_2Cu_3](PF_6)_3$ (two ligands capping a Cu_3 triangle) were identified by SCXRD analysis but were of poor quality. Compound **8a** provides low-quality twinned crystals for single-crystal X-ray diffraction (see below), but the corresponding compound $[(TMG_3trphen\text{-}Sb)_2Cu_2](B(C_6F_5)_4)_2\bullet 2$ MeCN (**8b**) with $B(C_6F_5)_4^-$ as counteranion provides single crystals of superior XRD quality from MeCN. Compound **8b** can be obtained from **8a** upon addition of 2 equiv of $KB(C_6F_5)_4$, or via the reaction of ligand **1** with 1.5 equiv of $[Cu(NCMe)_2][B(C_6F_5)_4]$[31] in MeCN.

We have also attempted to remove bridging chlorides from $[(TMG_3trphen\text{-}Sb)Cu_3(\mu\text{-}Cl)_3]$ (**3**) under various conditions. When $TlPF_6$ (3 equiv) was employed in MeCN, the resulting needle-shaped crystalline material proved to be the same as compound **8a**, albeit solvated by MeCN. On the other hand, the reaction of $AgPF_6$ (3 equiv) with compound **3** in MeCN, provided a poorly soluble and difficult to crystallize white solid, whose NMR signature was identical to that obtained from a reaction of ligand **1** with $AgPF_6$ in MeCN, thus indicating ligand transmetalation from Cu to Ag. We have been unable thus far to crystallize and fully characterize this product. We have also tried to use high-purity Ag(OTf) (3 equiv) for extracting chlorides from **3** in CH_2Cl_2, which led to the isolation of low yields of mononuclear $[(TMG_3H_3trphen\text{-}Sb)Cu(OTf)_3](OTf)$ (**10**), exhibiting protonation and detachment of the TMG arms, although the protonated ligand is still coordinated to Cu(I) via the Sb(III) element (Scheme 4). The supernatant affords an intractable mixture that also indicates partial ligand transformation. The provenance of protons, whether from the solvent or the ligand, is currently unknown, but notably, we have observed facile C−H activation of the NMe_2 residues in the past.[27] Instances in which metal triflate salts act as masked TfOH sources are also known in the literature.[32]

Finally, the reaction of 3 equiv of $KB(C_6F_5)_4$ with **3** in CH_2Cl_2 afforded an intriguing colorless product, $[(TMG_3trphen\text{-}Sb)Cu_3(\mu_3\text{-}Cl)_3Cu]_2[B(C_6F_5)_4]_2\bullet 10CH_2Cl_2$ (**11**), exhibiting partial chloride extraction (Scheme 5). While the crown-shaped $Cu_3(\mu\text{-}Cl)_3$ fragment is largely retained, extraction of Cu(I) sites is also evident, contributing to the assembly of a new $\{[Cu_3(\mu_3\text{-}Cl)_3]_2Cu_2\}$ core structure. The mechanism of formation is certainly complex, as we cannot generate the compound from the reaction of **3** with 2 equiv of $[Cu(NCMe)_2][B(C_6F_5)_4]$.

Scheme 4. Extraction of Chlorides from 3 by Silver Triflate

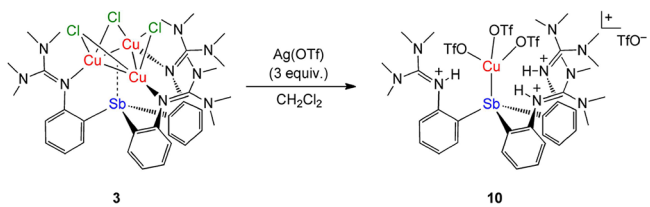

https://doi.org/10.1021/acs.organomet.3c00493
Organometallics 2024, 43, 634−652

Scheme 5. Partial Extraction of Chloride from [(TMG$_3$trphen-Sb)Cu$_3$(μ-Cl)$_3$] (3)

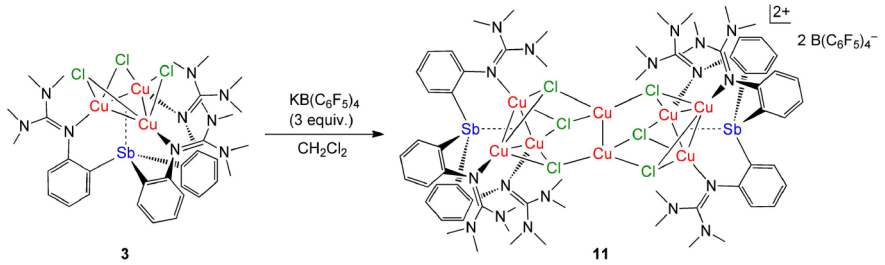

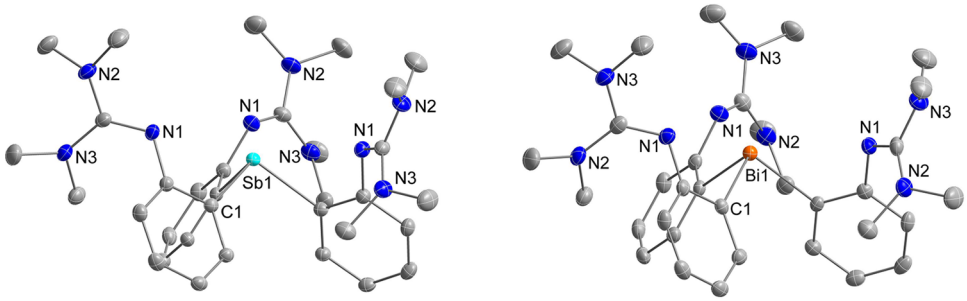

Figure 1. ORTEP Diagrams of TMG$_3$trphen-Sb•3CH$_2$Cl$_2$ (**1**), TMG$_3$trphen-Bi•3CH$_2$Cl$_2$ (**2**) drawn with 40% thermal ellipsoids. Selective interatomic distances [Å] and angles [°] for **1**: Sb(1)−C(1) = 2.169(5), C(1)−Sb(1)−C(1) = 95.09(18). For **2**: Bi(1)−C(1) = 2.2508(18), C(1)−Bi(1)−C(1) = 93.14(18).

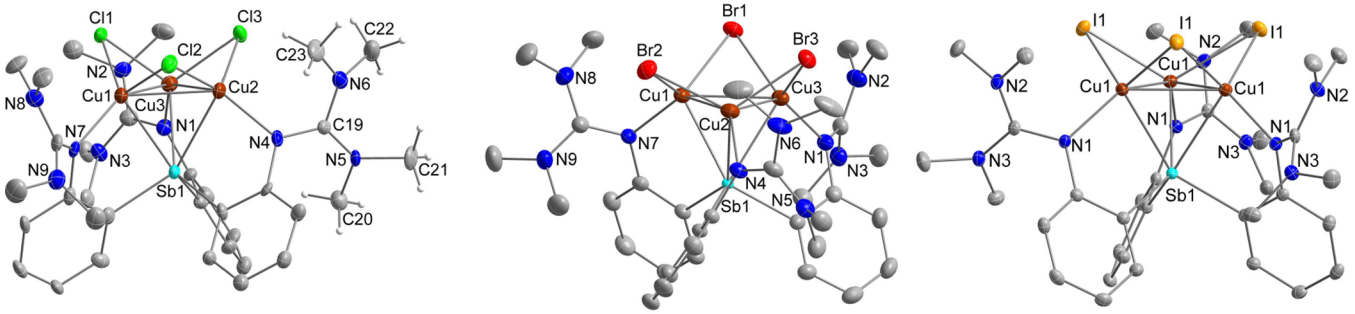

Figure 2. ORTEP diagrams of [(TMG$_3$trphen-Sb)Cu$_3$(μ-Cl)$_3$]•4CH$_2$Cl$_2$ (**3**), [(TMG$_3$trphen-Sb)Cu$_3$(μ-Br)$_3$]•4CH$_2$Cl$_2$ (**5**), [(TMG$_3$trphen-Sb)Cu$_3$(μ-I)$_3$]•3CH$_2$Cl$_2$ (**6**) drawn with 40% thermal ellipsoids. Selective interatomic distances [Å] and angles [°] for **3**: Sb(1)−Cu(1) = 2.652(2), Sb(1)−Cu(2) = 2.646(2), Sb(1)−Cu(3) = 2.673(2), Cu(1)−Cu(2) = 2.628(3), Cu(1)−Cu(3) = 2.594(3), Cu(2)−Cu(3) = 2.615(3), Cu(1)−Cl(1) = 2.320(4), Cu(1)−Cl(2) = 2.366(4), Cu(1)−N(7) = 2.027(11), Cu(2)−Cl(2) = 2.328(4), Cu(2)−Cl(3) = 2.337(4), Cu(2)−N(4) = 2.040(11), Cu(3)−Cl(1) = 2.342(4), Cu(3)−Cl(3) = 2.366(4), Cu(3)−N(1) = 2.001(11), Cu(2)−Cu(1)−Cu(3) = 60.11(7), Cu(1)−Cu(2)−Cu(3) = 59.29(7), Cu(1)−Cu(3)−Cu(2) = 60.60(7), Cu(1)−Cl(1)−Cu(3) = 67.60(11), Cu(1)−Cl(2)−Cu(2) = 68.09(12), Cu(2)−Cl(3)−Cu(3) = 67.57(11), Cu(1)−Sb(1)−Cu(2) = 59.48(6), Cu(1)−Sb(1)−Cu(3) = 58.29(6), Cu(2)−Sb(1)−Cu(3) = 58.91(6). For **5**: Sb(1)−Cu(1) = 2.6430(5), Sb(1)−Cu(2) = 2.6510(5), Sb(1)−Cu(3) = 2.6676(5), Cu(1)−Cu(2) = 2.6203(7), Cu(1)−Cu(3) = 2.5958(7), Cu(2)−Cu(3) = 2.6012(7), Cu(1)−Br(1) = 2.4502(6), Cu(1)−Br(2) = 2.4785(6), Cu(1)−N(7) = 2.032(3), Cu(2)−Br(2) = 2.4488(6), Cu(2)−Br(3) = 2.4523(6), Cu(2)−N(4) = 2.032(3), Cu(3)−Br(1) = 2.4670(6), Cu(3)−Br(3) = 2.4719(6), Cu(3)−N(1) = 2.020(3), Cu(2)−Cu(1)−Cu(3) = 59.822(18), Cu(1)−Cu(2)−Cu(3) = 59.621(18), Cu(1)−Cu(3)−Cu(2) = 60.557(18), Cu(1)−Br(1)−Cu(3) = 63.728(18), Cu(1)−Br(2)−Cu(2) = 64.252(18), Cu(2)−Br(3)−Cu(3) = 63.773(18), Cu(1)−Sb(1)−Cu(2) = 59.335(15), Cu(1)−Sb(1)−Cu(3) = 58.522(15), Cu(2)−Sb(1)−Cu(3) = 58.558(15). For **6**: Sb(1)−Cu(1) = 2.6619(5), Cu(1)−Cu(#1) = 2.6332(8), Cu(1)−I(1) = 2.6313(5), Cu(#1)−I(1) = 2.6410(5), Cu(1)−N(1) = 2.035(3), Cu(1)#1−Cu(1)−Cu(1)#2 = 60.0, Cu(1)−I(1)−Cu(1)#1 = 59.925(19), Cu(1)−Sb(1)−Cu(1)#1 = 59.289(17).

Solid-State Structures. Ligands TMG$_3$trphen-Sb (**1**) and TMG$_3$trphen-Bi (**2**) are essentially isostructural (Figure 1), featuring a rigorous C_3-symmetric geometry that places all three guanidinyl groups toward the same side as the endo located Sb/Bi element. This preorganized cavity provides similar coordination space for both ligands given the longer Bi−C edges but more acute angles for the BiC$_3$ pyramid.

Upon metalation with CuCl, both ligands extract a Cu$_3$(μ-Cl)$_3$ cluster in a manner similar to that previously noted in two rare cases, either with the assistance of ligand (o-(^{i}Pr$_2$P)-C$_6$H$_4$)$_3$E (E = Sb, Bi)[33] or with tris(2-(2-pyridyl)ethyl)-phosphine.[34] The resulting compounds (**3**, **4**) feature an approximate C_3-symmetric geometry and are distinguished by a crown-shaped Cu$_3$(μ-Cl)$_3$ unit embedded in the ligand framework. By contrast, the gas-phase structure of CuCl encompasses planar, D_{3h}-symmetric Cu$_3$Cl$_3$ rings (Cu−Cu = 2.627 ± 0.012, Cu−Cl = 2.166 ± 0.008 Å, and Cu−Cl−Cu = 73.9 ± 0.6°, at 689 K).[35]

For compounds **3** and **4** (Figures 2 and 3), the Cu$_3$(μ-Cl)$_3$ cluster is supported by a Sb(III) (**3**) or Bi(III) (**4**) axial

https://doi.org/10.1021/acs.organomet.3c00493
Organometallics 2024, 43, 634−652

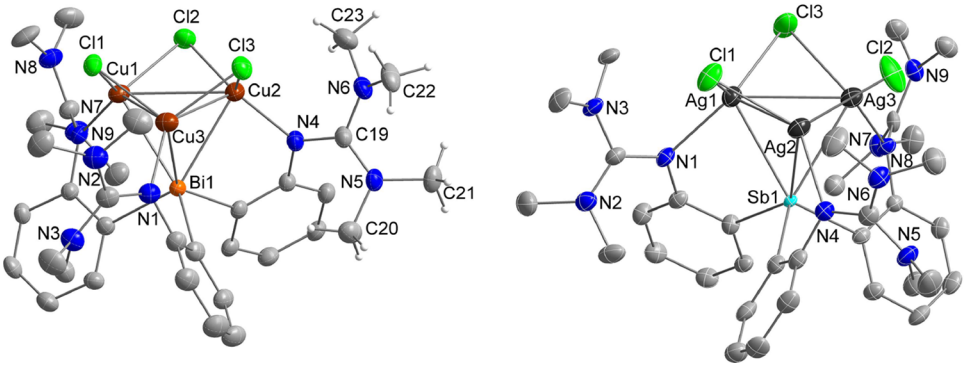

Figure 3. ORTEP diagrams of $[(TMG_3trphen\text{-}Bi)Cu_3(\mu\text{-}Cl)_3]\bullet 4CH_2Cl_2$ (**4**) and $[(TMG_3trphen\text{-}Sb)Ag_3(\mu\text{-}Cl)_3]\bullet 3CH_2Cl_2$ (**7**) drawn with 40% thermal ellipsoids. Selective interatomic distances [Å] and angles [°] for **4**: Bi(1)−Cu(1) = 2.7710(12), Bi(1)−Cu(2) = 2.7823(12), Bi(1)−Cu(3) = 2.8024(13), Cu(1)−Cu(2) = 2.8851(17), Cu(1)−Cu(3) = 2.8262(17), Cu(2)−Cu(3) = 2.8838(17), Cu(1)−Cl(1) = 2.259(3), Cu(1)−Cl(2) = 2.394(3), Cu(1)−N(7) = 2.021(7), Cu(2)−Cl(2) = 2.271(3), Cu(2)−Cl(3) = 2.339(3), Cu(2)−N(4) = 2.018(7), Cu(3)−Cl(1) = 2.360(3), Cu(3)−Cl(3) = 2.295(3), Cu(3)−N(1) = 2.015(8), Cu(2)−Cu(1)−Cu(3) = 60.64(4), Cu(1)−Cu(2)−Cu(3) = 58.67(4), Cu(1)−Cu(3)−Cu(2) = 60.69(4), Cu(1)−Cl(1)−Cu(3) = 75.42(8), Cu(1)−Cl(2)−Cu(2) = 76.36(8), Cu(2)−Cl(3)−Cu(3) = 76.95(8), Cu(1)−Bi(1)−Cu(2) = 62.60(4), Cu(1)−Bi(1)−Cu(3) = 60.94(3), Cu(2)−Bi(1)−Cu(3) = 62.18(4). For **7**: Sb(1)−Ag(1) = 2.9174(6), Sb(1)−Ag(2) = 2.9505(7), Sb(1)−Ag(3) = 2.9331(7), Ag(1)−Ag(2) = 2.9256(7), Ag(1)−Ag(3) = 2.9227(7), Ag(2)−Ag(3) = 2.8822(7), Ag(1)−Cl(1) = 2.6443(18), Ag(1)−Cl(3) = 2.509(2), Ag(1)−N(1) = 2.266(6), Ag(2)−Cl(1) = 2.5078(17), Ag(2)−Cl(2) = 2.630(2), Ag(2)−N(4) = 2.274(6), Ag(3)−Cl(2) = 2.524(2), Ag(3)−Cl(3) = 2.6209(19), Ag(3)−N(7) = 2.271(5), Ag(2)−Ag(1)−Ag(3) = 59.054(17), Ag(1)−Ag(2)−Ag(3) = 60.423(18), Ag(1)−Ag(3)−Ag(2) = 60.523(18), Ag(1)−Cl(1)−Ag(2) = 69.14(4), Ag(2)−Cl(2)−Ag(3) = 67.97(5), Ag(1)−Cl(3)−Ag(3) = 69.43(5), Ag(1)−Sb(1)−Ag(2) = 59.808(16), Ag(1)−Sb(1)−Ag(3) = 59.941(17), Ag(2)−Sb(1)−Ag(3) = 58.664(17).

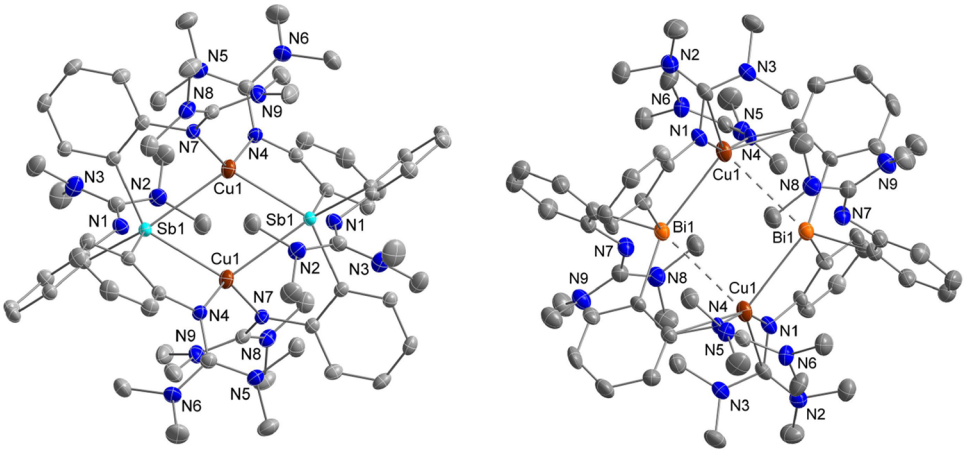

Figure 4. ORTEP diagrams of $[(TMG_3trphen\text{-}Sb)_2Cu_2][B(C_6F_5)_4]_2\bullet 2MeCN$ (**8b**) and $[(TMG_3trphen\text{-}Bi)_2Cu_2](PF_6)_2\bullet 2Et_2O$ (**9**) drawn with 40% thermal ellipsoids. Selective interatomic distances [Å] and angles [°] for **8b**: Sb(1)−Cu(1) = 2.5925(4), Sb(1)−Cu(1)#1 = 2.8121(4), Cu(1)−Cu(1)#1 = 3.0152(7), Cu(1)−N(4) = 2.060(2), Cu(1)−N(7) = 2.022(2), Cu(1)−Sb(1)−Cu(1)#1 = 67.681(13), N(4)−Cu(1)−Sb(1) = 88.00(6), N(4)−Cu(1)−Sb(1)#1 = 126.81(6), N(4)−Cu(1)−N(7) = 122.35(9), N(7)−Cu(1)−Sb(1) = 129.86(6), N(7)−Cu(1)−Sb(1)#1 = 82.21(6). For **9**: Bi(1)−Cu(1) = 2.9025(8), Bi(1)−Cu(1)#1 = 3.3075(8), Cu(1)−N(1) = 1.896(5), Cu(1)−N(4) = 1.896(5), Cu(1)−Bi(1)−Cu(1)#1 = 96.59(2), N(1)−Cu(1)−Bi(1) = 88.26(14), N(1)−Cu(1)−Bi(1)#1 = 120.96(16), N(1)−Cu(1)−N(4) = 155.0(2), N(4)−Cu(1)−Bi(1) = 112.73(15), N(4)−Cu(1)−Bi(1)#1 = 76.64(15).

element, capping all three Cu sites ($Sb-Cu_{3,cent}$ = 2.187, $Bi-Cu_{3,cent}$ = 2.241 Å), as well as by three guanidinyl residues, each coordinated to a separate edge of the Cu_3 triangle (ave. Cu−N = 2.023 ± 0.016 (**3**), 2.018 ± 0.003 (**4**) Å). The average Sb−Cu (2.657 ± 0.012 Å) and Bi−Cu (2.785 ± 0.013 Å) bond distances are shorter than those reported by Ke and Gabbaï (Sb−Cu = 2.802(2), Bi−Cu 2.934(2) Å) with (o-(^{i}Pr$_2$P)C$_6$H$_4$)$_3$E (E = Sb and Bi) ligands,[33] and very similar to the sum of covalent radii for Sb/Bi and Cu atoms (Sb−Cu = 2.71(6), Bi−Cu = 2.80(6) Å).[36]

The presence of cuprophilic (d^{10}−d^{10}) interactions[37] within the essentially equilateral Cu_3 triangle of the $Cu_3(\mu\text{-}Cl)_3$ unit is more nuanced, especially for the Bi supported compound **4**, since the observed Cu−Cu distances (2.612 ± 0.014 (**3**), 2.865 ± 0.027 (**4**) Å) are either within range (**3**) or exceed (**4**) the sum of covalent radii (Cu−Cu = 2.64(6) Å)[36] and may also be at the limit of the sum of the vdW radii (Cu−Cu = 2.80 Å), although the latter value may be an underestimation.[38] Similar metallophilic Cu−Cu interactions were suggested and computationally justified, in the previously reported cases of $[(o\text{-}(^i Pr_2P)C_6H_4)_3ECu_3(\mu\text{-}Cl)_3]$ (Cu−Cu = 2.660(2) (E = Sb), 2.853(2) (E = Bi) Å)[33] and $[(2\text{-}(2\text{-}Py)\text{-}CH_2CH_2)_3PCu_3(\mu\text{-}Cl)_3]$ (Cu−Cu = 2.542 ± 0.049 Å).[34] Single chloride bridges between pairs of Cu(I) sites (Cu−Cl = 2.343 ± 0.018 (**3**), 2.320 ± 0.049 (**4**) Å); Cu−Cl−Cu = 67.75 ± 0.24 (**3**), 76.24 ± 0.63 (**4**)°) complete the metal coordination sphere, with Cu−Cl distances that are very

https://doi.org/10.1021/acs.organomet.3c00493
Organometallics 2024, 43, 634−652

similar to those previously reported for the aforementioned $Cu_3(\mu\text{-}Cl)_3$ units.[33,34]

The bromo- and iodo-bridged congeners $[(TMG_3trphen\text{-}Sb)Cu_3(\mu\text{-}X)_3]$ (X = Br (**5**), I (**6**)) are essentially isostructural to the chloro analog **3**. Compound **6** features a strict C_3 axis penetrating the middle of the equilateral Cu_3 triangle and the apical Sb element (Figure 2). Interestingly, metrical parameters associated with their $[(L\text{-}Sb)Cu_3]$ framework (Cu−Cu = 2.6058 ± 0.0105 (**5**), 2.6332(8) (**6**), Sb−Cu = 2.6539 ± 0.0102 (**5**), 2.6619(5) (**6**) Å) are similar to those of **3**. The size of the halide is only reflected in the longer and slightly asymmetric halide bridges (Cu−Cl = 2.343 ± 0.018 (**3**), Cu−Br = 2.4615 ± 0.0116 (**5**), Cu−I = 2.6362 ± 0.0049 (**6**) Å) and the corresponding acute Cu−X−Cu angles (67.75 ± 0.24 (**3**), 63.918 ± 0.237 (**5**), 59.925(19) (**6**)°). The related Cu_3X_3 cluster embedded in tris(2-(2-pyridyl)ethyl)phosphine (L-P) exhibits a $[(L\text{-}P)Cu_3]$ framework that is more tightly coordinated (Cu−Cu ranges narrowly from 2.528 to 2.542 Å) but is highly asymmetric in the cases of X = Cl and I, since one Cu−P bond is longer than the other two by a significant margin (0.40 (Cl), 0.37 (I) Å).[34]

The $Ag_3(\mu\text{-}Cl)_3$ unit (**7**, Figure 3) is embedded in the cavity of ligand TMG_3trphen-Sb in a similar fashion to that observed for $Cu_3(\mu\text{-}Cl)_3$, as evidenced by the pseudo C_3-symmetric attachment of the cluster to the tripodal Sb ligand via the three guanidinyl residues (ave. Ag−N = 2.270 ± 0.003 Å) and the axial Sb (ave. Sb−Ag = 2.934 ± 0.014 Å). Within the $Ag_3(\mu\text{-}Cl)_3$ cluster, the average Ag−Ag (2.910 ± 0.020 Å) and Ag−Cl (2.573 ± 0.060 Å) bond distances are comparable to the sum of the corresponding covalent radii (Ag−Ag = 2.90(7), Ag−Cl = 2.47(6) Å)[36] and shorter than the values reported for two independent molecules in the unit cell of $[(o\text{-}(^iPr_2P)\text{-}C_6H_4)_3SbAg_3(\mu\text{-}Cl)_3]$ (Ag−Ag = 3.0288(8), 3.1559(8); Ag−Cl = 2.5791(14), 2.6443(16) Å).[33] One distinguishing feature of the $Ag_3(\mu\text{-}Cl)_3$ cluster is the somewhat asymmetric chloride bridging (Δ(Ag−Cl) = 0.118 ± 0.013 Å) presumably due to distortion arising from the accommodation of a larger cluster in the ligand cavity.

The structures of the halide-free compounds $[(TMG_3trphen\text{-}E)_2Cu_2](X)_2\bullet 2$ solv (E = Sb (**8a, 8b**), Bi (**9**); solv = THF (**8a**), MeCN (**8b**), Et_2O (**9**); X = PF_6 (**8a, 9**), $B(C_6F_5)_4$ (**8b**)) are all very similar (Figures 4 and S1), although significant differences in metrical parameters are observed. They all possess a Cu_2E_2 parallelogram with a short and a long Cu−E bond and exhibit a local inversion center applicable to the entire compound. Each stibine (**1**) or bismuthine (**2**) ligand is coordinated to both Cu sites via two separate TMG-substituted arms, whereas the third TMG residue remains noncoordinated, at a significant distance (>4 Å) from the closest Cu. The ligand moieties that bridge the shorter Cu−Sb bonds are oriented axially with respect to the Cu_2E_2 ring, whereas those spanning the longer Cu−Sb bonds are located equatorially. Since crystal data for **8a** were of low quality (derived from a twinned specimen), we rely on the solid-state structure of **8b** for further discussion of metrical parameters. Each symmetry-related Cu(I) site of **8b** is coordinated by two Sb(III) elements (Cu−Sb = 2.5925(4), 2.8121(4) Å; Sb−Cu−Sb = 112.319(13)°) and two N_{TMG} residues (Cu−N = 2.060(2), 2.022(2) Å; N−Cu−N = 122.35(9)°). Houser's four-coordinate geometry index, τ_4 (0.73),[39] places the coordination of the Cu(I) site between trigonal pyramidal and seesaw. The Cu···Cu interatomic distance (3.0152(7) Å) is rather long to denote any significant cuprophilic interaction. The bismuth analog **9** is geometrically equivalent to **8a**/**8b** yet the Cu_2Bi_2 parallelogram is characterized by metrical parameters (Cu−Bi = 2.9025(8), 3.3075(8) Å; Bi−Cu−Bi = 83.41(2)°) that include a bonafide covalent Cu−Bi bond and a longer Cu···Bi interaction that at best denotes a weak contact at the van der Waals sum of radii limit (3.47 Å).[38,40] The Cu···Cu interatomic bond distance (4.644 Å) also precludes any cuprophilic contacts. Therefore, the Cu(I) sites of **9** are essentially three-coordinate with shorter Cu−N bonds (both 1.896(5) Å) and more obtuse N−Cu−N angle (155.0(2)°) than those observed with the stibine analogs (**8a, 8b**).

A version of the coordination mode noted above was most recently unraveled in a comprehensive publication by Wright and co-workers[41] for $[\{(2\text{-}Me\text{-}8\text{-}quinolyl)_3Sb\}_2Cu_2](PF_6)_2$. In this case, the compound lacks an inversion center, and the Cu_2Sb_2 ring is essentially rhombic (Cu−Sb = 2.5451(19)−2.5884(19) Å) bridged by an ax/ax/eq/eq suite of ligand moieties rather than the alternating ax/eq/ax/eq motif observed in our work. Interestingly, the corresponding bismuth ligand $(2\text{-}Me\text{-}8\text{-}quinolyl)_3Bi$ did not provide compounds with Cu−Bi bonds.[41]

The structure of compound $[(TMG_3H_3trphen\text{-}Sb)Cu(OTf)_3](OTf)$ (**10**) (Figure S2) demonstrates an unusual decomplexation of the TMG residues of ligand **1** due to protonation (Cu−N interatomic distances vary from 3.561 to 3.902 Å), accompanied by retention of a strong Sb(III)−Cu(I) bond (2.4259(9) Å).[42] The pseudotetrahedral ligand field around the Cu(I) site also includes three coordinated triflates (Cu−O = 2.090 ± 0.012 Å) with less obtuse O−Cu−O (99.30 ± 2.60°) than Sb−Cu−O (118.37 ± 2.83°) angles, reflecting the repulsive effect of the Cu−Sb bond and the bulk of the protonated ligand.

Finally, compound $[(TMG_3trphen\text{-}Sb)Cu_3(\mu_3\text{-}Cl)_3Cu]_2[B(C_6F_5)_4]_2$ (**11**) (Figure 5) relates two $[(TMG_3trphen\text{-}Sb)Cu_3Cl_3]$ units via a central chloro-bridged Cu_2 element by means of inversion. This unique structure demonstrates metrical parameters for the essentially equilateral Cu^I_3 triangle and its coordination to the antimony ligand that are very similar to those demonstrated by **3**, save for the shorter Cu−N bond distances (Cu−N = 1.957 ± 0.044 Å) due to the weaker Cu−Cl bonds in **10**. The μ_2-Cl bridges in **3** become triply bridged in **10** by incorporating an additional Cu^I site from the central Cu_2 element. As a result, the Cu_3Cl_3 fragment in **10** exhibits longer Cu−Cl bond distances (2.413 ± 0.055 Å) and more acute Cu−Cl−Cu angles (65.27 ± 0.52°). Each Cu site of the Cu_2 dimer is coordinated by three chlorides in a trigonal planar arrangement (Cu−Cl = 2.272 ± 0.080 Å, Cl−Cu−Cl = 118.7 ± 9.9°) and also features a cuprophilic contact (Cu−Cu = 2.772(7) Å).

Summaries of crystallographic data for compounds **1**−**11** are collected in Tables S1−S4.

Solution Behavior. ^{1}H NMR data for compounds $[(TMG_3trphen\text{-}Sb)Cu_3(\mu\text{-}X)_3]$ (X = Cl (**3**), Br (**5**), I (**6**)) in CD_2Cl_2 at room temperature (298 K) exhibit broad peaks attributed to the four methyl groups of the TMG residues (fully resolved only for X = I), extending from δ 1.5 to 3.5 ppm for all compounds (Figure S3). The degree of resolution of the four distinct methyl peaks (all broad at 298 K) is enhanced with increasing size of the halide presumably due to restricted rotation of the TMG branches. Low-temperature ^{1}H NMR data (243−298 K, Figure S4) indicate that all four methyl groups are progressively resolved with decreasing temperature,

https://doi.org/10.1021/acs.organomet.3c00493
Organometallics 2024, 43, 634−652

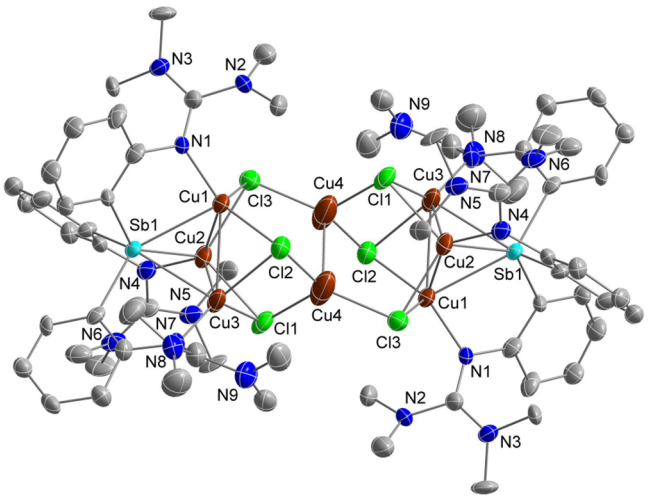

Figure 5. ORTEP diagram of $[(TMG_3trphen\text{-}Sb)Cu_3(\mu_3\text{-}Cl)_3Cu]_2[B(C_6F_5)_4]_2\bullet 10CH_2Cl_2$ (**11**) drawn with 40% thermal ellipsoids. Selective interatomic distances [Å] and angles [°]: Sb(1)−Cu(1) = 2.661(3), Sb(1)−Cu(2) = 2.649(3), Sb(1)−Cu(3) = 2.645(3), Cu(1)−Cu(2) = 2.648(4), Cu(1)−Cu(3) = 2.601(4), Cu(2)−Cu(3) = 2.564(4), Cu(4)−Cu(4)#1 = 2.772(7), Cu(1)−Cl(2) = 2.328(5), Cu(1)−Cl(3) = 2.465(6), Cu(1)−N(1) = 2.004(12), Cu(2)−Cl(1) = 2.386(5), Cu(2)−Cl(3) = 2.398(5), Cu(2)−N(4) = 1.968(14), Cu(3)−Cl(1) = 2.404(5), Cu(3)−Cl(2) = 2.497(6), Cu(3)−N(7) = 1.899(14), Cu(4)−Cl(1) = 2.375(7), Cu(4)−Cl(2) = 2.261(6), Cu(4)−Cl(3) = 2.180(6), Cu(2)−Cu(1)−Cu(3) = 58.48(11), Cu(1)−Cu(2)−Cu(3) = 59.83(10), Cu(1)−Cu(3)−Cu(2) = 61.69(9), Cu(2)−Cl(1)−Cu(3) = 64.72(14), Cu(2)−Cl(1)−Cu(4) = 103.8(2), Cu(3)−Cl(1)−Cu(4) = 74.62(19), Cu(1)−Cl(2)−Cu(3) = 65.12(15), Cu(1)−Cl(2)−Cu(4) = 101.9(2), Cu(3)−Cl(2)−Cu(4) = 74.8(2), Cu(1)−Cl(3)−Cu(2) = 65.97(14), Cu(1)−Cl(3)−Cu(4)#1 = 101.9(2), Cu(2)−Cl(3)−Cu(4)#1 = 97.9(2), Cu(4)#1−Cu(4)−Cl(1) = 82.2(2), Cu(4)#1−Cu(4)−Cl(2) = 98.8(2), Cu(4)#1−Cu(4)−Cl(3) = 105.0(2).

to afford four sharp peaks at −30 °C (for **3**: δ (ppm, CD_2Cl_2, −30 °C) = 3.100 (H(23)), 2.758 (H(21/22)), 2.582 (H(21/22), 1.672 (H(20), see Figure 2 for atom labeling). Peak assignments were facilitated by computational (B3LYP/6-311+G(2d,p)) single point NMR property determination at the B3LYP/6-31G(d)-optimized geometry of **3**, which indicates that the most upfield peak is due to protons residing in the shielded region of the phenylene rings, whereas the most downfield peak arises from protons pointing *endo* with respect to the ligand cavity. With respect to $[(TMG_3trphen\text{-}Bi)Cu_3(\mu\text{-}Cl)_3]$ (**4**), a featureless broad band at room temperature progressively resolves to four distinct Me peaks at −30 °C in CD_2Cl_2. A similar broad band, assigned to TMG methyl groups, is also observed for $[(TMG_3trphen\text{-}Sb)Ag_3(\mu\text{-}Cl)_3]$ (**7**). Apparently, for this more sizable ligand cavity, the rotational restrictions for the TMG arms are more relaxed than those applying to compounds **1**−**3** at room temperature. Notably, the ^{1}H NMR spectra of the $[(TMG_3trphen\text{-}Sb)_2Cu_2]^{2+}$ compounds (**8a, 8b**) exhibit only a single peak for all Me groups of the three TMG arms (as well as equivalent aryl groups) in CD_3CN at 298 K. On the other hand, the corresponding $[(TMG_3trphen\text{-}Bi)_2Cu_2]^{2+}$ (**9**) compound distinguishes the TMG arms (and the related aryl groups) in a 2:1 ratio, most likely reflecting the coordinated (two arms) and noncoordinated (one arm) TMG moieties observed in the solid-state structure of **9**. Fast exchange between coordinated and noncoordinated TMG groups may account for the single TMG peak observed with the Sb analogs (**8a**, **8b**), although dissociation to monomers with possible MeCN coordination cannot be excluded. The protonation of the TMG arms in compound **10** can easily be detected by ^{1}H NMR. Finally, compound **11** demonstrates a ^{1}H NMR spectrum not unlike that of **3** at 298 K, featuring broad overlapping peaks for the Me groups of TMG.

The metal coordination of the strongly superbasic TMG arms results in charge delocalization over the CN_3 unit, as demonstrated by the essentially equivalent C−N bond distances (SCXRD data) and downfield shift of the central C peak (>160 ppm, ^{13}C NMR data).

Computational Studies. The structures of **3** and **4** were optimized and found to have an overall generally good agreement with the experimental crystallographic data. EDA calculations[43] were conducted to decompose the interaction energy and give a more detailed view of the bonding for these complexes (Table 1). The results show that complexes **3** and **4** have similar bonding energetic patterns, as evidenced by the same percent contribution of attraction interactions and energy values. The leading attractive interaction is electrostatic interaction between two charge-neutral moieties, mainly arising from the Cu−N coordination bonds between two fragments. The steric effect of Sb (**3**) and Bi (**4**) to the Cu_3Cl_3 fragment accounts for the Pauli repulsion seen in both complexes, whereas the transfer of electrons synergistically increases their electrostatic attraction. Also, the Sb complex **3** has a slightly larger electrostatic (−287.8 kcal/mol) and orbital interaction energies (−141.7 kcal/mol) vs those for Bi complex **4** (−275.8 kcal/mol and −133.5 kcal/mol, respectively). The higher orbital interaction energy in the Sb complex **3** vs the Bi analogue **4**, an attractive force, is offset by the correspondingly higher Pauli repulsion energy, resulting in the Bi complex **4** possessing a stronger overall interaction energy than that in the Sb analogue **3**.

As the Cu−N coordination bonds are broken during the fragmentation procedure for the EDA analysis, the total ΔE_{int} does not directly reflect the interaction strengths between the Cu_3Cl_3 and ligand with Sb/Bi moieties. To overcome this limitation, we further divide ΔE_{OrbInt} into pairwise interactions to reveal the detailed bonding pictures between fragments under the ETS-NOCV theoretical framework.[43] The broken-down ΔE_{OrbInt} is denoted as $\Delta E_{OrbInt,i}$ (i = integer) in the energy strength order. NOCV results are consistent with Sb/Bi → Cu_3 dative bonding in both complexes **3** and **4**. The NOCV

Table 1. Energy Decomposition Analysis Results of Compounds 3 and 4[a]

compound	ΔE_{elstat}	ΔE_{Pauli}	ΔE_{OrbInt}	ΔE_{disp}	ΔE_{int}
3	−287.8 (63%)	344.5	−141.7 (31%)	−24.4 (6%)	−109.4
4	−275.8 (63%)	323.5	−133.5 (31%)	−25.4 (6%)	−111.2

[a]Unit: kcal/mol, values in parentheses are the energy percentage to the total attractive interaction. Total interaction energy (ΔE_{int}) is decomposed into electrostatic interaction (ΔE_{elstat}), Pauli repulsion (ΔE_{Pauli}), orbital interaction (ΔE_{OrbInt}), and dispersion energy (ΔE_{disp}).

https://doi.org/10.1021/acs.organomet.3c00493
Organometallics 2024, 43, 634−652

pairwise orbital deformation density maps are illustrated in Figure 6; the electron flows from the white region to the brown region comprising the bonding formation. The largest contributing NOCV pairwise orbitals ($\Delta E_{OrbInt,1}$) of **3** and **4** are the bonding interactions between Sb or Bi, respectively, and the Cu_3Cl_3 moieties, with interaction energies of −32.6 kcal/mol and −23.6 kcal/mol, respectively. The electrons that contribute to the bonding behavior originate from the filled Sb 5s or Bi 6s orbitals to the admixed Cu $4s^{0+x}/3d^{10-x}$ partially unoccupied/partially occupied orbitals, confirming the directional Sb/Bi→Cu_3 dative bonding character (Figure 6a/c). The $\Delta E_{OrbInt,2-4}$ values for **3** and **4** clearly suggest Cu−N coordination bonds (Figure 6b/d), with comparable attractive bond strengths of −40.3 and −43.6 kcal/mol, respectively. The rest of the NOCV pairwise orbitals possess negligible interaction energies (<4 kcal/mol in total) suggest that the major bonding in these species is due to the Cu−N coordination, followed by Sb/Bi→Cu_3 donor contributions. Any residual backdonation (Sb/Bi→Cu_3) cannot be excluded at the present time, but this contribution is likely to be very small.

The independent gradient model based on the Hirshfeld partition (IGMH)[44] analyzes noncovalent interactions between Sb/Bi and Cu_3Cl_3 moieties (Figure 7). The results correspond to the above NOCV results in that a stronger interfragment bonding character exists in **3** and **4**. The plots confirm the attractive interaction between Sb/Bi atoms and Cu atoms, as illustrated by the blue region in Figure 7a−d. Comparing the IGMH results of **3** and **4**, the blue color between Sb and Cu_3 is deeper than that between Bi and Cu_3, which suggests a stronger interaction in **3**, in agreement with the larger interaction energy between Sb → Cu_3 as indicated by the NOCV results (Figure 6a/c). These calculations are consistent with a decrease in electron-donating ability of the pnictine lone pair from Sb to Bi, concomitant with an increase in s-character. Also, the calculated average bond distance of 2.924 Å for Bi−Cu as compared to the average bond distance of 2.746 Å for Sb−Cu (2.68−2.84 Å) suggests that a slightly shorter bond contributes to the Sb → Cu_3 interaction, given the rather similar van der Waals radii of Sb (2.06 Å) and Bi (2.07 Å).[40]

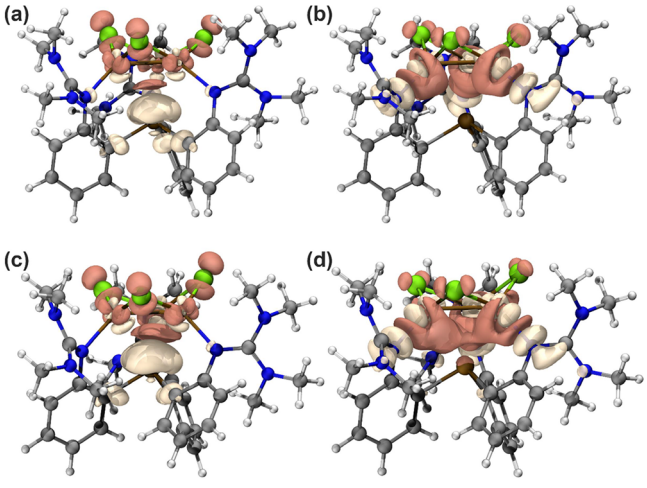

Figure 6. NOCV deformation density maps of (a/c) $\Delta E_{OrbInt,1}$ and (b/d) $\Delta E_{OrbInt,2-4}$ of **3** and **4**, respectively. Isovalue: 0.002 au **3** (for (a) $\Delta E_{OrbInt,1}$ = −32.6 kcal/mol; for (b) $\Delta E_{OrbInt,2-4}$ = −40.3 kcal/mol), **4** (for (c) $\Delta E_{OrbInt,1}$ = −23.6 kcal/mol; for (d) $\Delta E_{OrbInt,2-4}$ = −43.6 kcal/mol).

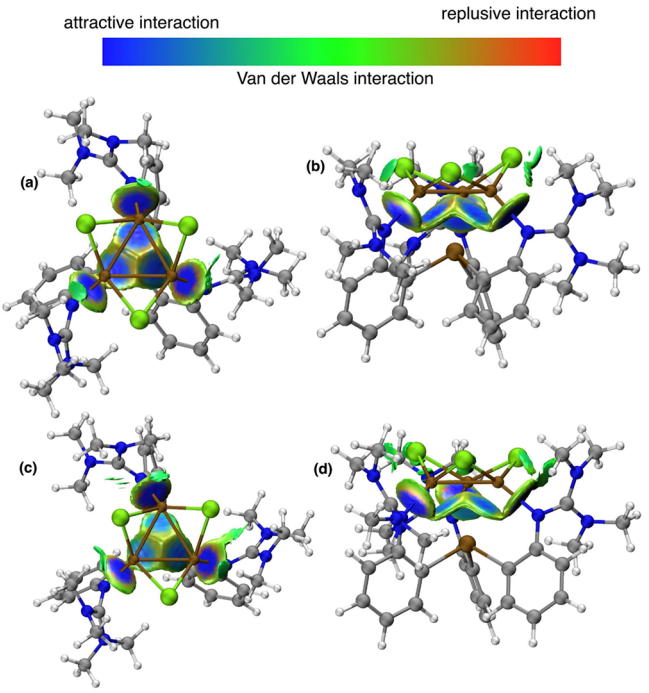

Figure 7. Independent gradient model based on Hirshfeld partition (IGMH) analysis results of **3** and **4** in (a/c) top view and (b/d) side view, respectively. The value of the surface is set as 0.01 au.

Catalytic and Mechanistic Nitrene-Transfer Studies. *Aziridination of para-Substituted Styrenes.* An initial evaluation of nitrene addition to olefins was conducted with the assistance of imidoiodinane PhINTs (1 equiv, Ts = tosyl) and a panel of para-substituted styrenes (8 equiv) in the presence of different catalytic systems (5 mol % with respect to Cu) at 30 °C (drybox temperature) over 12 h (Table 2). The choice of the solvent (MeCN) was suggested by an initial screening of various chlorinated and nonchlorinated solvents (MeCN, benzene, CH_2Cl_2, 1,2-dichloroethane, and chlorobenzene) in catalytic reactions with styrene/PhINTs mediated by [(TMG$_3$trphen-Sb)$Cu_3(\mu$-Cl)$_3$] (**3**). Acetonitrile has an edge over all other solvents, even if the catalyst is more soluble in CH_2Cl_2. Molecular sieves (5 Å) are also needed for obtaining good yields, thus denoting sensitivity to any adventitious water.

Gratifyingly, both catalysts **3** and **4** provide good to excellent yields of the corresponding aziridines as evaluated by ^{1}H NMR spectra of the purified products (with respect to an internal standard). Both **3** (87%) and **4** (62%) can be recovered at the end of the reaction, albeit to a much lower extent for **4**, potentially reflecting the fragility of the Bi−C bond.[45]

To evaluate the effect of partial removal of chlorides as suggested by the synthesis of compound **11** (see above), KPF_6 (3 equiv) was added to the catalytic mixture containing [(TMG$_3$trphen-Sb)$Cu_3(\mu$-Cl)$_3$] (**3**). Yields of aziridines (Table 2) are not unlike those obtained in the absence of KPF_6, save for the most electron-withdrawing styrenes (CF_3, NO_2), for which unusually high yields are observed. Interestingly, $SbAg_3(\mu$-Cl)$_3$ reagent **7** is totally unproductive.

Aziridination of Other Alkenes. The more robust catalyst **3** was further employed in the aziridination of a wider panel of aromatic and aliphatic olefins under the conditions noted

https://doi.org/10.1021/acs.organomet.3c00493
Organometallics 2024, 43, 634−652

Table 2. Yields of Aziridination Products of para-Substituted Styrenes Catalyzed by [(TMG$_3$trphen-E)Cu$_3$(μ-Cl)$_3$] (E = Sb (3), Bi (4))[a]

Entry No.	Substrate	Products		Yield (%) [(L-Sb)Cu$_3$Cl$_3$](3)	Yield (%) 3/KPF$_6$ (3 equiv.)	Yield (%) [(L-Bi)Cu$_3$Cl$_3$] (4)
1.	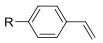	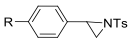	R = H	92	80	85
2.			R = Me	73	77	80
3.			R = ^{t}Bu	77	63	82
4.			R = OMe	28	polymer	polymer
5.			R = O^{t}Bu	53	polymer	polymer
6.			R = F	77	74	83
7.			R = Cl	88	79	89
8.			R = CF$_3$	87	96	82
9.			R = NO$_2$	83	87	73

[a]Conditions: catalyst, 0.0125 mmol with respect to Cu (5 mol %); PhINTs, 0.25 mmol; olefin, 2.0 mmol; KPF_6, 0.0125 mmol; MS 5 Å, 20 mg; solvent (MeCN) 0.250 g; 30 °C; 12 h.

above (Table 3). In the presence of ortho styrene substitution (entry 1), significantly lower yields are obtained, due to steric and electronic reasons (orthogonal orientation of the aromatic/olefinic planes).[46] Benzylic amination was not observed in this case. Nitrene transfer to α-substituted styrenes (Me, Ph; entries 2, 3) is also sterically hampered, especially for the α-Ph congener. The α-methylstyrene affords substantial allylic amination in almost 1:1 ratio with respect to aziridination (entry 2). Surprisingly, the major product for α-phenylstyrene is a hydroxyamine rather than the more common enamine (entry 3), even under conditions that are purported to exclude water. In this case, aziridine is known to undergo facile ring opening (and rearrangement).[47] The corresponding cis- and trans-β-substituted styrenes (Me, Ph; entries 4−7) are less hampered by sterics and afford good yields of the corresponding cis- and trans-aziridines. A minor amount of allylic amination is only observed for the Me-substituted analog. On the other hand, the retention of stereochemistry for aziridination of the mechanistically diagnostic cis-β-R-styrenes is rather modest (cis:trans = 1:1.3, R = Me; 1.8:1, R = Ph). Amination of allylic/benzylic C−H sites is very competitive with styrenyl aziridinations (entries 8, 9), provided that acyclic trans substrates are involved (entry 8) that usually restrict aziridination yields. Allylic aminations are also dominant with cycloalkenes (entries 10, 11), although the more electron-rich cyclooctene (entry 12) favors aziridination by a significant margin since H atom abstraction from the allylic C−H bonds is associated with large energy barriers, due to modest $\sigma_{C-H}/\pi_{C=C}$ orbital overlap.[48] Other aliphatic alkenes (entries 13−15) exhibit significantly lower yields than those encountered with aromatic congeners.

Amination of Benzylic Substrates. The more challenging amination of C−H-bond containing substrates was subsequently examined. The benchmark substrate ethylbenzene (1 equiv) was initially explored with PhINTs (2 equiv) in the presence of catalytic amounts of [(TMG$_3$trphen-Sb)Cu$_3$(μ-Cl)$_3$] (**3**) (5 mol % with respect to Cu) in several solvent matrices. Under all circumstances, benzylic amination yields did not exceed 10%. The more electrophilic nitrene source PhINTces (Tces = 2,2,2-trichloroethoxysulfonyl) provided significantly better yields and was further applied in the amination of ethylbenzene. An initial screening of chlorinated and nonchlorinated solvents indicated that PhCl and $PhCF_3$ are the most productive solvents, especially if a small amount of HFIP (10%) is added. Presynthesized PhINTces[49] is significantly more soluble than PhINTs but is unstable in halogenated solvents. The selection of $PhCF_3$/HFIP (10:1 v/v) for further experimentation was indicated by the superior stability it offered to PhINTces at 30 °C over a period of 24 h in the absence of light, according to ^{1}H NMR experiments.

The amination of a panel of benzylic substrates (Table 4) was pursued most effectively with a 2:1 ratio of PhINTces/substrate in $PhCF_3$/HFIP (10:1 v/v) at 30 °C, over 24 h. Several catalysts (5 mol % with respect to Cu) were explored, namely, [(TMG$_3$trphen-Sb)Cu$_3$(μ-X)$_3$] (X = Cl (**3**), Br (**5**), I (**6**)), [(TMG$_3$trphen-Bi)Cu$_3$(μ-Cl)$_3$] (**4**), and [(TMG$_3$trphen-Sb)$_2$Cu$_2$](PF$_6$)$_2$ (**8a**). As a general characteristic, all catalysts afford moderate to good amination yields specifically for sec-benzylic sites. Prim-benzylic C−H bonds are unaffected (entry 11), as are C−H bonds adjacent to O/N atoms and tert/sec/prim C−H bonds of unactivated alkanes and cycloalkanes (yields ≤10%, not shown). Notably, amination of ethylbenzene does not occur in the presence of catalytic amounts (5 mol %) of TMG$_3$trphen-Sb (**1**) or CuCl alone.

A cursory look at the yields afforded for the amination of all benzylic sites shown in Table 4 by catalysts **3** and **4** indicates that no significant variations exist in the operation of these axially supported Sb and Bi reagents. This is likely consistent with nitrene docking in the Cu$_3$ plane (cis with respect to the E−Cu$_{3,cent}$ axis) rather than on the encumbered side of the halide crown. Inspection of the solid-state structures of **3** and **4** provides evidence of ample coordination space externally to the Cu$_3$ ring (in-plane). Additionally, the difference between Sb(III) and Bi(III) in terms of electron donicity to the Cu$_3$ cluster may be insufficient to significantly alter the metal-nitrene electrophilicity.

The amination yields for the functionalization of the benzylic substrates by catalysts [(TMG$_3$trphen-Sb)Cu$_3$(μ-X)$_3$] (X = Cl (**3**), Br (**5**), I (**6**)) vary more appreciably (Table 4). For the panel of the para-substituted ethylbenzenes (entries 1−9), each catalyst provides good yields not only with substrates bearing ED substituents (entries 1−3) but also with para-X (X = F, Cl, Br, I) substituted congeners (entries 4−7), a trend that usually denotes significant benzyl radical stabilization via resonance effects. Only strongly EW substituents (entries 8, 9) are associated with low yields, as anticipated for electrophilic metal nitrene-driven reactions. The yields for the amination of sec-benzylic sites (entry 10) are modest most

https://doi.org/10.1021/acs.organomet.3c00493
Organometallics 2024, 43, 634−652

Table 3. Yields of Aziridination/Amination Products of Various Olefins Catalyzed by $[(TMG_3trphen\text{-}Sb)Cu_3(\mu\text{-}Cl)_3]$ (3)[a]

Entry No.	Substrate	Products	Yields (%)
1.	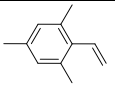	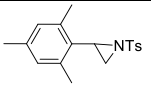	22
2.	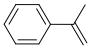	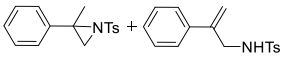	24, 23
3.	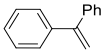	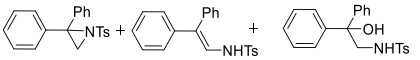	tr, 2, 17
4.		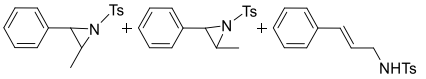	28, 36, 3
5.	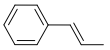	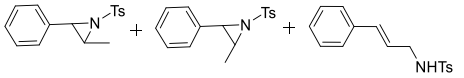	49, 2, 4
6.		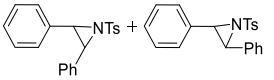	30, 17
7.	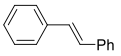	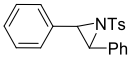	45
8.	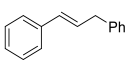	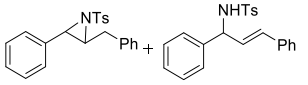	25, 37
9.		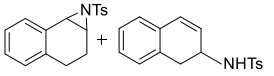	48, nd
10.		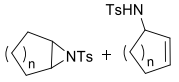	n = 1	4, 14
11.			n = 2	2, 42
12.			n = 4	51, nd
13.		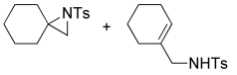	8, 5
14.		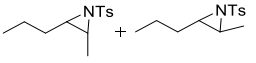	19, 12
15.	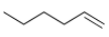	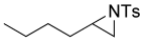	28

[a]Conditions: 3, 0.0125 mmol with respect to Cu (5 mol %); PhINTs, 0.25 mmol; olefin, 2.0 mmol; MS 5 Å, 20 mg; solvent (MeCN) 0.250 g; 30 °C; 12 h.

likely due to steric encumbrance, and those for prim-benzylic sites (entry 11) are below ≤10% given the higher aliphatic C−H bond energy of toluene (90 kcal/mol[50]). Steric hampering is also reflected in the moderate yields for the benzylic amination of 1,2,3,4-tetrahydronaphthalene and derivatives (entries 12, 13). Competitions between benzylic and tert-C−H sites (entries 14, 15) singularly result in benzylic aminations with yields increasing with increasing distance between the two sites. Finally, acetate not only deactivates adjacent C−H sites (entry 16), as anticipated, but curiously seems to interfere with the operation of the Br- and I-possessing catalysts **5** and **6**. Lateral comparisons between catalysts **3**, **5**, and **6** do not reveal any particular trends possibly because the effect of the halide is likely to be multivariate in regulating (i) the electrophilicity of the putative metal nitrene; (ii) the approach of the substrate to the active catalytic site; and (iii) the stability offered to any substrate-centered carboradical (or carbocation) upon H atom abstraction. Finally, the halide-free catalyst $[(TMG_3trphen\text{-}Sb)_2Cu_2](PF_6)_2$ (**8a**) affords similar yields and trends to those encountered with the aforementioned reagents but also shows signs of more tolerance to steric encumbrance and/or electron-withdrawing functionalities (entries 14−16).

Direct comparisons to the halide-rich reagents **3**−**6** cannot be made at the present time given the structural uniqueness of catalyst **8a**. On average, the previously explored catalyst $[(TMG_3trphen)Cu](PF_6)$,[27] featuring N_{amine} apical coordination, is more active than the present reagents, but this may be due to its mononuclear character. Incidentally, an interesting mechanistic distinction between Cu(I) catalysts that carry halide ligands and others that are halide-free, has been recently reported by Pérez and co-workers.[51]

Hammett Plots. To start placing these reagents in a mechanistic context, Hammett plots were constructed for the competitive amination (PhINTces) of ethylbenzene versus

https://doi.org/10.1021/acs.organomet.3c00493
Organometallics 2024, 43, 634−652

Table 4. Yields of Benzylic Amination of Various Substrates Mediated by $[(TMG_3trphen\text{-}Sb)Cu_3(\mu\text{-}X)_3]$ (X = Cl (3) Br (5), I (6)), $[(TMG_3trphen\text{-}Bi)Cu_3(\mu\text{-}Cl)_3]$ (4), and $[(TMG_3trphen\text{-}Sb)_2Cu_2](PF_6)_2$ (8a)[a]

Entry No.	Substrate	Product	Yield (%) $[(L\text{-}Sb)Cu_3X_3]$ X = Cl (3)	X = Br (5)	X = I (6)	Yield (%) $[(L\text{-}Bi)Cu_3Cl_3]$ (4)	Yield (%) $[(L\text{-}Sb)_2Cu_2]^{2+}$ (8a)
1.			50	35	49	49	46
2.		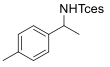	54	41	42	41	32
3.	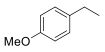	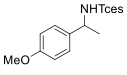	60	29	56	50	41
4.		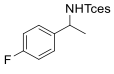	48	44	42	50	49
5.		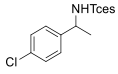	49	67	63	43	54
6.		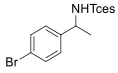	61	39	37	57	45
7.		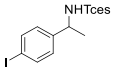	52	46	31	51	41
8.	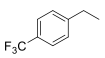	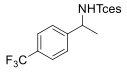	13	18	10	20	13
9.	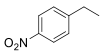	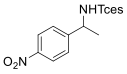	31	12	17	26	9
10.		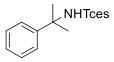	12	31	34	20	26
11.		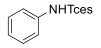	5	7	2	6	8
12.		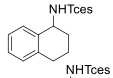	23	34	36	31	20
13.	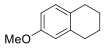	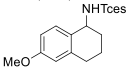	26	50	36	29	26
14.	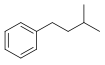	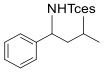	30	22	25	24	23
15.			7	9	10	13	25
16.	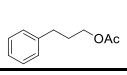	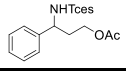	26	2	5	25	25

[a]Conditions: catalyst, 0.0125 mmol with respect to Cu (5 mol %); PhINTces, 0.50 mmol; benzylic substrate, 0.25 mmol; MS 5 Å, 20 mg; solvent ($PhCF_3$/HFIP 10:1 v/v), 0.300 g (0.500 g for **8a**); 30 °C; 24 h.

seven para-X-ethylbenzenes (X = MeO, Me, F, Br, I, CF_3, and NO_2) as mediated by catalyst **3** (5 mol % with respect to Cu) in $PhCF_3$/HFIP (10:1 v/v) at 30 °C (5 h). Reasonably, good linear free-energy correlations of log (k_X/k_H) versus the polar substituent parameter σ_p ($\rho_p = -1.70$, $R^2 = 0.95$) and, even better, versus the resonance-sensitive σ^+ ($\rho^+ = -1.22$, $R^2 = 0.98$) can be obtained (Figure 8 and Table S5). The negative ρ_p and ρ^+ coefficients indicate that significant positive charge develops en route to the transition state, presumably at the benzylic carbon, by means of an incipient hydrogen-atom abstraction by an electrophilic oxidant. These sizable ρ values are more consistent with stepwise benzylic C−H functionalization ($[Ru_2(hp)_4Cl]$, $\rho^+ = -0.90$; $[Ru_2(esp)_2SbF_6]$, $\rho^+ = -1.49$)[52] by comparison to the more modest values found in Rh amination chemistry (−0.47,[17g] −0.55,[17b] −0.66,[53] −0.73,[17a] −0.90[17f]); the latter is characterized by a concerted asynchronous C−H insertion pathway.

CONCLUSIONS

The following are the major findings and insights of the present study:

1. The synthesized tripodal ligands $TMG_3trphen$-E (E = Sb (**1**) and Bi (**2**)) generate extended cavities that permit capturing of $M_3(\mu\text{-}X)_3$ fragments (M = Cu, Ag; X = Cl, Br, I) extracted from anhydrous MX precursors. Single-

https://doi.org/10.1021/acs.organomet.3c00493
Organometallics 2024, 43, 634−652

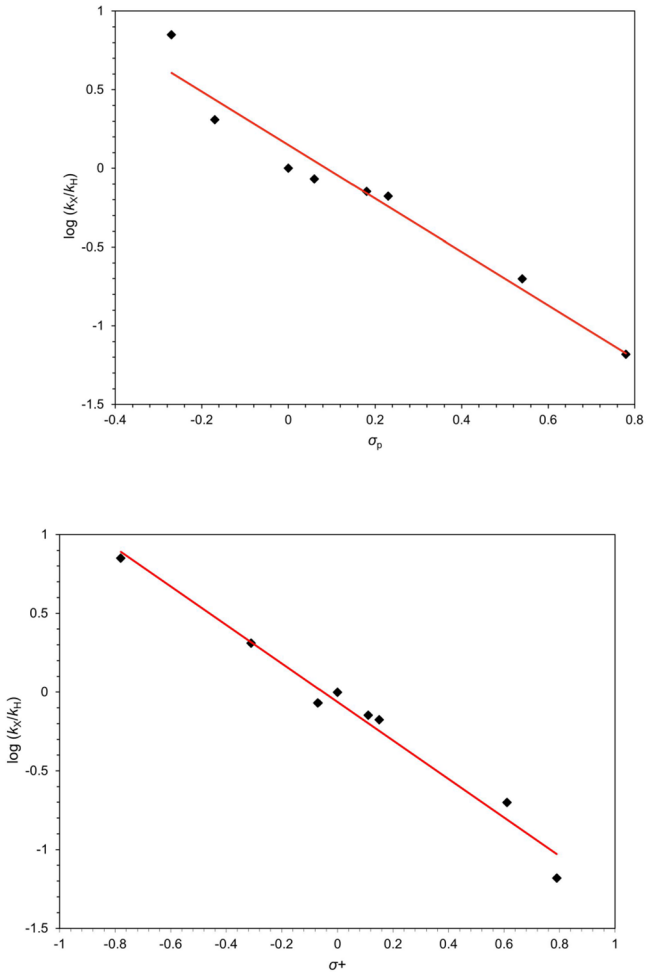

Figure 8. Linear free energy correlation of $\log(k_X/k_H)$ as a function of σ_p (left) ($\rho_p = -1.70$, $R^2 = 0.95$) and σ^+ (right) ($\rho^+ = -1.22$, $R^2 = 0.98$) for the competitive amination of para-substituted ethylbenzenes versus ethylbenzene catalyzed by $[(TMG_3trphen\text{-}Sb)Cu_3(\mu\text{-}Cl)_3]$ (**3**).

crystal crystallographic analysis indicates that the crown-shaped $M_3(\mu\text{-}X)_3$ units are supported by axial Sb(III) and Bi(III) elements, triply bridging the M_3 triangle, and equatorial N-donor residues provided by the superbasic TMG ligand arms. ^{1}H NMR data suggest that the rotation of the CN_3 branches of TMG is partially restricted at ambient temperatures to various degrees, commensurate with the bulk of the halide, with resolution of all four methyl groups emerging at low temperatures.

2. Although abstraction of the halides in select cases can best be achieved by means of $TlPF_6$, the most convenient path for obtaining halide-free copper(I) compounds with ligands **1** and **2** involves the use of $[Cu(NCMe)_4](PF_6)$ or $[Cu(NCMe)_2][B(C_6F_5)_4]$. The resulting complexes $[(TMG_3trphen\text{-}E)_2Cu_2]^{2+}$ (E = Sb and Bi) are dimeric in the solid state and possess an asymmetric $Cu_2(\mu\text{-}E)_2$ core that is retained in solution for E = Bi and tentatively for E = Sb, according to ^{1}H NMR data. Other efforts to dechlorinate $[(TMG_3trphen\text{-}Sb)Cu_3(\mu\text{-}Cl)_3]$ by means of $AgPF_6$ and AgOTf lead to ligand transmetalation and protonation, respectively. Partial dechlorination and cluster rearrangement is achieved with $KB(C_6F_5)_4$.
3. Energy decomposition analysis (EDA) studies performed on $[(TMG_3trphen\text{-}E)Cu_3(\mu\text{-}Cl)_3]$ (E = Sb (**3**) and Bi (**4**)) indicate that among the attractive interactions, the electrostatic component contributions (63%) far exceed those associated with orbital interactions (31%) and dispersion energy (6%) for both compounds. The natural orbitals for chemical valence (NOCV) analysis, further supported by the independent gradient model based on Hirshfeld partition (IGMH) method, suggest that the dominant orbital interaction is that between the Cu(I) sites and N_{TMG} residues, followed by the Sb/Bi → Cu_3 donor interaction between the Sb 5s or Bi 6s orbitals and admixed Cu $4s^{0+x}/3d^{10-x}$ orbitals. The attractive Sb → Cu_3 interaction is more pronounced than that of Bi, given the increased s-character of the 6s lone pair. Little, if any, π-backdonation can be extracted from the analysis, suggesting that **1** and **2** are largely L-type ligands.[54]
4. An initial evaluation of $[(TMG_3trphen\text{-}E)Cu_3(\mu\text{-}Cl)_3]$ (E = Sb (**3**), Bi (**4**)) as nitrene-transfer agents in the aziridination of various p-substituted styrenes by PhINTs afforded very good to excellent product yields, although catalyst **4** showed signs of fragility. Further evaluation of **3** as the catalyst for the aziridination of other aromatic and aliphatic alkenes provided good to modest yields and selectivities, respectively, in response to steric (aromatic alkenes) and electronic (aliphatic alkenes) challenges.
5. The amination of C−H bonds is best accomplished by the more electrophilic PhINTces in $PhCF_3$/HFIP (10:1 v/v). An extensive study of catalysts $[(TMG_3trphen\text{-}E)Cu_3(\mu\text{-}X)_3]$ (E = Sb, X = Cl (**3**) Br (**5**), I (**6**)); E = Bi, X = Cl (**4**) and $[(TMG_3trphen\text{-}Sb)_2Cu_2](PF_6)_2$ (**8a**) demonstrates good yields, almost exclusively for the amination of electron-rich and unencumbered sec-benzylic-C−H bonds (mostly para-substituted ethylbenzenes). Although no discernible patterns of reactivity emerge that can be correlated with catalyst characteristics, reagents **3** and **8a** are more consistent in their behavior. Their activity is still inferior to the previously explored $[(TMG_3trphen)Cu](PF_6)$ catalyst[27] presumably because the latter catalyst is strictly mononuclear. Hammett plots for the competitive p-X-ethylbenzene/ethylbenzene amination (PhINTces) mediated by **3**, provide evidence that a stepwise C−H activation takes place by an electrophilic oxidant, featuring an intermediate benzylic carboradical.

Future studies will address more precisely the interaction between these reagents and the N-donor sources, to explore the location of nitrene docking and further establish the mode of operation of the resulting active oxidant responsible for C−H aminations. In addition, catalyst modifications that are purported to incorporate halide substituents in the ligand framework will be pursued, given the known role of halide substituents in *Z*-type ligands.[29,55]

EXPERIMENTAL SECTION

Safety Warning. Antimony and thallium compounds can be highly toxic and should be handled and disposed carefully.

Synthesis and Characterization of Ligands and Metal Compounds. *$TMG_3trphen\text{-}Sb\bullet 3CH_2Cl_2$ (**1**).* 2-(2′-bromophenyl)-1,1,3,3-tetramethylguanidine (1.10 g, 4.08 mmol) was dissolved in 20

https://doi.org/10.1021/acs.organomet.3c00493
Organometallics 2024, 43, 634−652

mL of Et_2O in a Schlenk flask. The solution was cooled in a dry ice/acetone bath to −78 °C, after which a cyclohexane solution of *sec*-butyllithium (1.4 M, 6.4 mL, 8.99 mmol) was added, effecting a color change to bright orange. After stirring for 1 h while being kept cold, $SbCl_3$ (0.307 g, 1.34 mmol) dissolved in THF (10 mL) was added at −78 °C via cannula. The reaction mixture was kept at −78 °C for 2 h and then was allowed to warm to room temperature and stirred overnight. After the addition of 1.0 mL of methanol, the volatiles were removed in vacuo, producing a yellow-orange residue. The crude was dissolved in EtOAc (20 mL) and washed with water (10 mL). The aqueous phase was extracted with additional EtOAc (20 mL). The combined organic phases were dried over sodium sulfate and concentrated by rotary evaporation to give an oily mass. The oily mass was dissolved in 10 mL of CH_2Cl_2 and chilled to 0 °C for 1 h, separating colorless crystals. The white solid was collected by filtration, washed with cooled CH_2Cl_2 (5 mL), and dried in vacuum (yield = 0.580 g, 62%). ^{1}H NMR (CD_3CN, 1.94 ppm): δ 7.08 (t, 3H, aryl), 6.97(d, 3H, aryl), 6.60 (t, 3H, aryl), 6.41(d, 3H, aryl), 2.57 (s, 36H, CH_3).^{13}C NMR (CD_3CN, 118.26, 1.32 ppm): δ 159.0, 157.5, 137.6, 135.3, 129.1, 120.6, 120.2, 39.9. IR (KBr, cm^{-1}): ν 3031, 2932, 2889, 1539,1452, 1419, 1378, 1136, 1018, 791, 723, 535. UV−vis (CH_3CN): λ_{max} (ε (M^{-1} cm^{-1})) 220(76263). Elem. Anal. calcd for $C_{36}H_{54}Cl_6N_9Sb$ (**1**): C, 45.64; H, 5.75, N, 13.31. Found: C, 45.71; H, 5.76, N, 13.29.

*TMG_3trphen-Bi•3CH_2Cl_2 (**2**).* 2-(2′-bromophenyl)-1,1,3,3-tetramethylguanidine (1.16 g, 4.31 mmol) was dissolved in 20 mL of THF in a Schlenk flask. The solution was cooled in a dry ice/acetone bath to −78 °C, after which a cyclohexane solution of *sec*-butyllithium (1.4 M, 6.8 mL, 9.48 mmol) was added, effecting a color change to bright orange. After stirring for 1 h while being kept cold, $BiCl_3$ (0.448 g, 1.42 mmol), dissolved in THF (10 mL), was added at −78 °C via cannula. The reaction mixture was kept at −78 °C for 2 h and then was allowed to warm to room temperature. The reaction mixture was refluxed for 16 h, and subsequently, the solvent was removed to give an oily residue that was redissolved in toluene (20 mL). The reaction mixture was heated again and stirred at 90−95 °C for 3 h. The temperature of the reaction was lowered to ambient conditions, and the solvent was evacuated to dryness to give an oily mass. The residual oily mass was suspended in CH_2Cl_2 (10 mL) and was stirred vigorously at room temperature for 30 min, separating white crystals that were collected by filtration (yield = 0.550 g, 49%). ^{1}H NMR (CD_3CN, 1.94 ppm): δ 7.49 (d, 3H, aryl), 7.09 (t, 3H, aryl), 6.65 (t, 3H, aryl), 6.51(d, 3H, aryl), 2.58 (s, 36H, CH_3) ^{13}C NMR (CD_3CN, 118.26, 1.32 ppm): δ 159.2, 157.6, 139.5, 128.5, 122.7, 120.7, 39.9. IR (KBr, cm^{-1}): ν 3031, 2918, 2791, 1545, 1443, 1419, 1372, 1133, 1012, 781, 747, 724, 534. UV−vis (CH_3CN): λ_{max} (ε (M^{-1} cm^{-1})) 214 (59181). Elem. Anal. calcd for $C_{36}H_{54}BiCl_6N_9$ (**2**): C, 41.79; H, 5.26, N, 12.18. Found: C, 41.73; H, 5.23, N, 12.12.

*[(TMG_3trphen-Sb)Cu_3(μ-Cl)$_3$]•4CH_2Cl_2 (**3**).* To a suspension of CuCl (138 mg, 1.39 mmol) in THF (12 mL) was added a solution of TMG_3trphen-Sb (**1**) (321 mg, 0.463 mmol) in THF (18 mL) at room temperature. The solution was stirred for 24 h. The volatiles were removed under vacuum, and the residue was redissolved in CH_2Cl_2 (10 mL) and stirred for 6 h. The solution was filtered and concentrated to give an off-white-colored powder (yield = 0.380 g, 83%). The compound was recrystallized from CH_2Cl_2 to obtain X-ray-quality crystals. ^{1}H NMR (CD_2Cl_2, 5.32 ppm, 243 K): δ 7.17−7.14 (t, 3H, aryl), 7.02−7.01 (d, 3H, aryl), 6.69−6.66 (t, 3H, aryl), 6.46−6.44 (d, 3H, aryl), 3.10(s, 9H, CH_3), 2.76 (s, 9H, CH_3), 2.58 (s, 9H, CH_3), 1.67 (s, 9H, CH_3). ^{13}C NMR (CD_2Cl_2, 54.0 ppm): δ 166.2, 156.3, 136.5, 131.7, 126.0, 122.0, 121.7, 40.4, 30.6. IR (KBr, cm^{-1}): ν 3476, 3044, 2929, 2879, 2791, 1519, 1453, 1405, 1392, 1330, 1266, 1155, 1027, 853, 750, 725, 536. UV−vis (CH_2Cl_2): λ_{max} (ε (M^{-1} cm^{-1})) 235 (225820). Elem. Anal. calcd for $C_{33}H_{48}Cl_3Cu_3N_9Sb$ (**3** − 4CH_2Cl_2): C, 40.05; H, 4.89, N, 12.74. Found: C, 39.99; H, 4.84, N, 12.80.

*[(TMG_3trphen-Bi)Cu_3(μ-Cl)$_3$]•4CH_2Cl_2 (**4**).* To a suspension of CuCl (57.2 mg, 0.58 mmol) in THF (12 mL) was added a solution of TMG_3trphen-Bi (**2**) (150 mg, 0.192 mmol) in THF (18 mL) at room temperature. The solution was stirred for 24 h. The volatiles were removed under vacuum, and the residue was redissolved in 1,2-dichloroethane (10 mL) and stirred for 6 h. The solution was filtered and concentrated to give off-white colored powder (yield = 0.205g, 99%). The compound was recrystallized from CH_2Cl_2 to obtain X-ray-quality crystals. ^{1}H NMR (CD_2Cl_2, 5.32 ppm, 243 K): δ 7.50−7.48 (d, 3H, aryl), 7.21−7.18 (t, 3H, aryl), 6.80−6.77 (t, 3H, aryl), 6.58−6.56 (d, 3H, aryl), 3.19(s, 9H, CH_3), 2.82 (s, 9H, CH_3), 2.61 (s, 9H, CH_3), 1.69 (s, 9H, CH_3).^{13}C NMR (CD_2Cl_2, 54.0 ppm): δ 162.5, 150.2, 143.4, 127.7, 121.9, 118.5, 115.7, 40.7, 39.9. IR: 3040, 2924, 2878,2114, 1518, 1447, 1415, 1406, 1388, 1330, 1260, 1234, 1199, 1152, 1109, 1064, 1041, 1025, 923, 850, 805, 751, 720, 536. UV−vis (CH_2Cl_2): λ_{max} (ε (M^{-1} cm^{-1})) 235 (26520). Elem. Anal. calcd for $C_{33}H_{48}BiCl_3Cu_3N_9$ (**4** − 4CH_2Cl_2): C, 36.81; H, 4.49, N, 11.71. Found: C, 36.77; H, 4.45, N, 11.78.

*[(TMG_3trphen-Sb)Cu_3(μ-Br)$_3$]•4CH_2Cl_2 (**5**).* To a suspension of CuBr (205 mg, 1.43 mmol) in THF (12 mL) was added a solution of TMG_3trphen-Sb (**1**) (330 mg, 0.477 mmol) in THF (18 mL) at room temperature. The solution was stirred for 24 h. The volatiles were removed under vacuum, and the residue was redissolved in CH_2Cl_2 (10 mL) and stirred for 6 h. The solution was filtered and concentrated to give off-white colored powder (yield = 0.402 g, 85%). The compound was recrystallized in CH_2Cl_2 to obtain X-ray-quality crystals. ^{1}H NMR (CD_2Cl_2, 5.32 ppm, 243 K): δ 7.25−7.21 (t, 3H, aryl), 7.08−7.07 (d, 3H, aryl), 6.75−6.71 (t, 3H, aryl), 6.51−6.49 (d, 3H, aryl), 3.20(s, 9H, CH_3), 2.85 (s, 9H, CH_3), 2.65 (s, 9H, CH_3), 1.74 (s, 9H, CH_3). ^{13}C NMR (CD_2Cl_2, 54.0 ppm): δ 165.9, 156.0, 136.0, 130.9, 121.5, 120.7, 40.8, 15.0. IR (KBr, cm^{-1}): ν 3043, 2924, 2881,2792, 1517,1453,1416, 1404, 1392, 1330, 1282, 1265, 1202, 1155, 1116, 1063, 1047, 1028, 926, 854, 807, 753, 726, 705, 537, 452. UV−vis (CH_2Cl_2): λ_{max} (ε (M^{-1} cm^{-1})) 230 (225450). Elem. Anal. calcd for $C_{33}H_{48}Br_3Cu_3N_9Sb$ (**5** − 4CH_2Cl_2): C, 35.30; H, 4.31, N, 11.23. Found: C, 35.34; H, 4.34, N, 11.19.

*[(TMG_3trphen-Sb)Cu_3(μ-I)$_3$]•3CH_2Cl_2 (**6**).* To a suspension of CuI (372 mg, 1.95 mmol) in THF (12 mL) was added a solution of TMG_3trphen-Sb (**1**) (450 mg, 0.650 mmol) in THF (18 mL) at room temperature. The solution was stirred for 24 h. The volatiles were removed under vacuum and the residue was redissolved in CH_2Cl_2 (10 mL) and stirred for 6 h. The solution was filtered and concentrated to give off-white colored powder (yield = 0.530 g, 82%). The compound was recrystallized from CH_2Cl_2 to obtain X-ray-quality crystals. ^{1}H NMR (CD_2Cl_2, 5.32 ppm, 243 K): δ 7.22−7.18 (t, 3H, aryl), 7.05−7.03 (d, 3H, aryl), 6.73−6.69 (t, 3H, aryl), 6.45−6.43 (d, 3H, aryl), 3.19(s, 9H, CH_3), 2.84 (s, 9H, CH_3), 2.61 (s, 9H, CH_3), 1.70 (s, 9H, CH_3). ^{13}C NMR (CD_2Cl_2, 54.0 ppm): δ 166.6, 156.3, 136.1, 130.7, 121.5, 120.3, 40.7, 14.8. IR (KBr, cm^{-1}): ν 3042, 2923,2880, 2792, 1557,1544, 1512, 1454, 1415, 1404, 1392, 1329, 128. UV−vis (CH_2Cl_2): λ_{max} (ε (M^{-1} cm^{-1})) 340(18032). Elem. Anal. calcd for $C_{33}H_{48}Cu_3I_3N_9Sb$ (**6** − 3CH_2Cl_2): C, 31.36; H, 3.83, N, 9.97. Found: C, 31.38; H, 3.85, N, 9.93.

*[(TMG_3trphen-Sb)Ag_3(μ-Cl)$_3$]•3CH_2Cl_2 (**7**).* To a solution of TMG_3trphen-Sb (**1**) (186 mg, 0.268 mmol) in THF (20 mL), AgCl (115 mg, 0.805 mmol) was added at room temperature. The suspension was stirred for 2 weeks, protected from light. The volatiles were removed under vacuum, and the residue was redissolved in CH_2Cl_2 (20 mL) and stirred for 12 h. The solution was filtered and concentrated to give off-white colored powder (yield = 0.215 g, 71%). The compound was recrystallized from CH_2Cl_2 to obtain X-ray-quality crystals. ^{1}H NMR (CD_2Cl_2, 5.32 ppm, 243 K): δ 7.25−7.22 (t, 3H, aryl), 7.13−7.11 (d, 3H, aryl), 6.77−6.73(t, 3H, aryl), 6.52−6.50 (d, 3H, aryl), 2.66 (s, 36H, CH_3). ^{13}C NMR (CD_2Cl_2, 54.0 ppm): 165.1, 156.6, 137.2, 130.9, 122.1, 120.8, 39.8, 29.6. IR (KBr, cm^{-1}): ν 3020, 2930, 2870, 1519, 1454, 1417, 1406, 191, 1263, 1153, 1026, 852, 758, 725, 536. UV−vis (CH_2Cl_2): λ_{max} (ε (M^{-1} cm^{-1})) 295(12534). Elem. Anal. calcd for $C_{33}H_{48}$ $Ag_3Cl_3N_9Sb$ (**7** − 3CH_2Cl_2): C, 35.31; H, 4.31, N, 11.23. Found: C, 35.36; H, 4.33, N, 11.19.

*[(TMG_3trphen-Sb)$_2Cu_2$](PF_6)$_2$•2THF (**8a**).* A solution of [Cu(CH_3CN)$_4$](PF_6) (108 mg, 0.288 mmol) in acetonitrile/THF (5 mL each) was added to a prestirred solution of TMG_3trphen-Sb (**1**) (200 mg, 0.288 mmol) in acetonitrile (20 mL) at room temperature.

https://doi.org/10.1021/acs.organomet.3c00493
Organometallics 2024, 43, 634−652

The suspension was stirred for 24 h. The reaction mixture was filtered, reduced to 5 mL, and stored at −35 °C for 2 weeks to obtain X-ray quality crystals (yield = 0.145 g, 51%). ^{1}H NMR (CD_3CN, 1.94 ppm): δ 7.45−7.44 (d, 6H, aryl), 7.17−7.13 (t, 6H, aryl), 6.80−6.76 (t, 6H, aryl), 6.42−6.39 (d, 6H, aryl), 2.67 (s, 72H, CH_3). ^{13}C NMR (CD_3CN, 118.26, 1.32 ppm): 163.9, 157.0, 137.2, 131.6, 130.0, 122.3, 121.6, 120.9, 40.1. IR: 3672, 2935, 2883, 1515, 1454, 1416, 1394, 1324, 1281, 1265, 1231, 1201, 1142, 1111, 1062, 1046, 1021, 875, 834, 783, 762, 750, 726, 710, 556, 536, 467, 448. UV−vis (CH_3CN): λ_{max} (ε (M^{-1} cm^{-1})) 275(70831). Elem. Anal. calcd for $C_{66}H_{96}Cu_2F_{12}N_{18}P_2Sb_2$ (**8a** − 2THF): C, 43.99; H, 5.37, N, 13.99. Found: C, 44.02; H, 5.38, N, 13.92.

*[(TMG$_3$trphen-Sb)$_2$Cu$_2$][B(C$_6$F$_5$)$_4$]$_2$•2MeCN (**8b**).* An acetonitrile solution (10 mL) of [Cu(CH_3CN)$_2$][B(C_6F_5)][31] (64.4 mg, 0.078 mmol) was added to a prestirred solution of TMG_3trphen-Sb (**1**) (36.05 mg, 0.052 mmol) in acetonitrile (10 mL) at room temperature. The suspension was stirred for 24 h. The reaction mixture was filtered, reduced to 5 mL under vacuum, and stored at −35 °C for 1 week to obtain X-ray quality colorless crystals (yield = 0.054 g, 70%). ^{1}H NMR (CD_3CN, 1.94 ppm): δ 7.50−7.46 (d, 6H, aryl), 7.19−7.15(t, 6H, aryl), 6.82−6.78 (t, 6H, aryl), 6.44−6.42 (d, 6H, aryl), 2.69 (s, 72H, CH_3). ^{13}C NMR (CD_3CN, 118.26, 1.32 ppm): δ 165.07, 157.0, 137.1, 129.5, 121.9, 121.7, 120.3, 52.1, 39.7. IR (cm^{-1}): 2932, 1643, 1513, 1460, 1420, 1396, 1324, 1274, 1156, 1085, 1021, 978, 850, 807, 774, 755, 727, 683, 661, 611, 574, 537. UV−vis (CH_3CN): λ_{max} (ε (M^{-1} cm^{-1})) 215(147250). Elem. Anal. calcd for $C_{118}H_{102}B_2Cu_2F_{40}N_{20}Sb_2$ (**8b**): C, 48.01; H, 3.48, N, 9.49. Found: C, 48.07; H, 3.50, N, 9.45.

*[(TMG$_3$trphen-Bi)$_2$Cu$_2$](PF$_6$)$_2$•2Et$_2$O (**9**).* A solution of [Cu(CH_3CN)$_4$](PF_6) (143.4 mg, 0.385 mmol) in acetonitrile (5 mL) was added to a prestirred solution of TMG_3trphen-Bi (**2**) (200 mg, 0.256 mmol) in acetonitrile (20 mL) at room temperature. The suspension was stirred for 24 h. The reaction mixture was filtered, reduced to 5 mL under vacuum, and carefully layered with diethyl ether to obtain X-ray quality crystals at −35 °C over a period of 2 weeks (yield = 0.035 g, 6.4%). ^{1}H NMR (CD_3CN, 1.94 ppm): δ 7.85−7.83 (d, 2H, aryl), 7.26−7.22 (t, 6H, aryl), 7.19−7.15 (t, 2H, aryl), 6.95−6.91 (t, 4H, aryl), 6.88−6.84 (d, 2H, aryl), 6.83−6.80 (d, 6H, aryl), 6.56−6.54 (d, 2H, aryl), 2.75 (s, 42H, CH_3), 2.67(s, 30H, CH_3). ^{13}C NMR (CD_3CN, 118.26, 1.32 ppm): 164.9, 157.0, 139.3, 130.0, 129.3, 124.0, 123.1, 122.1, 40.3. IR: 3677, 3367, 2937, 1630, 1526, 1485, 1472, 1451, 1424, 1398, 1322, 1263, 1233, 1205, 1158, 1066, 1038, 831, 750, 696, 606, 556, 442. UV−vis (CH_3CN): λ_{max} (ε (M^{-1} cm^{-1})) 265(58035). Elem. Anal. calcd for $C_{66}H_{96}Bi_2Cu_2F_{12}N_{18}P_2$ (**9** − 2Et_2O): C, 40.11; H, 4.90, N, 12.76. Found: C, 40.08; H, 4.88, N, 12.80.

*[(TMG$_3$H$_3$trphen-Sb)Cu(OTf)$_3$](OTf)•1.21CH$_2$Cl$_2$ (**10**).* A methylene chloride solution (15 mL) of [(TMG$_3$trphen-Sb)Cu$_3$(μ-Cl)$_3$] (**3**) (64.1 mg, 0.065 mmol) was added to solid Ag(OTf) (49.93 mg, 0.195 mmol), and the reaction was stirred for 12 h in the absence of light. The resulting mixture was filtered to remove AgCl and reduced to 5.0 mL under vacuum. The clear solution was kept at −35 °C over a period of 1 week, affording large colorless crystals of the titled compound (yield = 0.036 g, 14%; based on Cu). ^{1}H NMR (CD_2Cl_2, 5.32 ppm): δ 7.36−7.32 (t, 3H, aryl), 7.25−7.23 (d, 3H, aryl), 6.93−6.89 (t, 3H, aryl), 6.61−6.59 (d, 3H, aryl), 2.85 (bs, 36H, CH_3), 1.26 (s, 3H, = NH). ^{13}C NMR (CD_2Cl_2, 54.0 ppm): 166.5, 155.6, 136.5, 132.5, 128.0, 122.6, 122.0, 40.7, 30.2. IR: 3225, 3053, 2930, 1630, 1547, 1520, 1456, 1419, 1398, 1328, 1262, 1222, 1154, 1028, 855, 753, 636, 517, 447. UV−vis (CH_2Cl_2): λ_{max} (ε (M^{-1} cm^{-1})) 235(10664). Elem. Anal. calcd for $C_{37}H_{51}CuF_{12}N_9O_{12}S_4Sb$ (**10** − 1.21CH_2Cl_2): C, 32.79; H, 3.79, N, 9.30. Found: C, 32.75; H, 3.78, N, 9.35.

*[(TMG$_3$trphen-Sb)Cu$_3$(μ$_3$-Cl)$_3$Cu]$_2$[B(C$_6$F$_5$)$_4$]$_2$•10CH$_2$Cl$_2$ (**11**).* A methylene chloride solution (20 mL) of [(TMG$_3$trphen-Sb)Cu$_3$(μ-Cl)$_3$] (**3**) (47.0 mg, 0.047 mmol) was added to K[B(C_6F_5)$_4$] (102.3 mg, 0.142 mmol), and the reaction mixture was stirred for 24 h. The resulting mixture was filtered to remove KCl and reduced to 5.0 mL under vacuum. The solution was kept at −35 °C over a period of 1 week, to provide off-white crystals of the titled compound (yield = 0.046 g, 75%; based on Cu). ^{1}H NMR ($CDCl_3$, 7.26 ppm): δ 7.27−7.24 (t, 6H, aryl), 7.19−7.17 (d, 6H, aryl), 6.85−6.82 (t, 6H, aryl), 6.49−6.47 (d, 6H, aryl), 3.15 (bs, 12H, CH_3), 2.81 (bs, 40H, CH_3), 1.90 (bs, 20H, CH_3). ^{13}C NMR ($CDCl_3$, 77.2 ppm): 166.0, 155.4, 137.8, 135.4, 132.2, 122.4, 121.5, 53.9, 40.0. IR: 2928, 1643, 1513, 1457, 1420,1407, 1396, 1330, 1270, 1233, 1158, 1085, 1031, 977, 854, 809,774, 755, 725, 683,661, 611, 574, 537, 450. UV−vis (CH_3CN): λ_{max} (ε (M^{-1} cm^{-1})) 230(14172). Elem. Anal. calcd for $C_{114}H_{96}B_2Cl_6Cu_8F_{40}N_{18}Sb_2$ (**11** − 10CH_2Cl_2): C, 39.53; H, 2.79, N, 7.28. Found: C, 39.49; H, 2.78, N, 7.31.

Catalytic and Mechanistic Studies. *General Catalytic Olefin Aziridination Procedure.* In a typical experiment, a 20 mL screw-cap vial containing a small magnetic bar was charged in sequence with the catalyst (0.0125 mmol with respect to Cu), N-(p-tolylsulfonyl)-imido]phenyliodinane (93.3 mg, 0.25 mmol), molecular sieves (5 Å) (20 mg), olefin (2.0 mmol), and solvent (0.200 g) (acetonitrile, unless otherwise stated). The reaction mixture was stirred vigorously at 30 °C for 24 h (unless otherwise stated). After completion of the reaction, the products were isolated by column chromatography (silica gel) and quantified by ^{1}H NMR (in $CDCl_3$) versus an internal standard (4′-methoxyacetophenone). All aziridination and/or allylic/benzylic amination products are known compounds and have been identified with the assistance of ^{1}H by comparison to spectroscopic features reported for authentic samples in the literature.

General Catalytic Benzylic Amination Procedure. In a standard method for copper-catalyzed amination, a tiny magnetic stirrer was placed in a flame-dried 20 mL screw cap vial. To this vial, catalyst (0.0125 mmol with respect to copper), 2,2,2-trichloroethyl(phenyl-λ_3-iodanylidene)sulfamate (PhINTces) (214.4 mg, 0.500 mmol), and molecular sieves (5 Å) (20 mg) were added sequentially. A solution of the substrate (0.250 mmol) in a mixture of trifluorotoluene and HFIP (10:1 v/v, 300 mg) was added to the vial that contained the solids. The reaction was stirred at 30 °C for 24 h. After completion of the reaction, the products were isolated by column chromatography (silica gel) using a mixture of hexane and ethyl acetate and were quantified by ^{1}H NMR (in $CDCl_3$) versus an internal standard (4′-methoxyacetophenone).

Hammett Plots. The general procedure for the amination of benzylic substrates was conducted with the assistance of the catalyst [(TMG$_3$trphen-Sb)Cu$_3$(μ-Cl)$_3$]•4CH_2Cl_2 (**3**) (0.0125 mmol with respect to Cu). The reaction mixture was composed of 1.0 mmol of ethylbenzene, 1.0 mmol of *p*-X-ethylbenzene (X = Me, MeO, F, Cl, Br, CF_3, and NO_2), and PhINTces (2 mmol) in the $PhCF_3$:HFIP mixture (10:1 v/v). The reaction vial was sealed tightly and wrapped with aluminum foil to protect the reaction mixture from light. The reactions were stirred for 6 h. At the end of the reaction, the mixture was flash chromatographed on silica gel (CH_2Cl_2) in order to recover the benzylic aminated products and evaluate their ratio by quantitative ^{1}H NMR analysis in $CDCl_3$.

■ ASSOCIATED CONTENT

Supporting Information

The Supporting Information is available free of charge at https://pubs.acs.org/doi/10.1021/acs.organomet.3c00493.

General considerations; synthesis and characterization; X-ray crystallography; catalytic and mechanistic studies; computational methods; crystallographic data; competitive amination reactions; ORTEP; and ^{1}H and ^{13}C NMR (PDF)

Atomic coordinates of compound **4** (XYZ)

Atomic coordinates of compound **3** (XYZ)

Accession Codes

CCDC 2309022−2309033 contain the supplementary crystallographic data for this paper. This data can be obtained free of charge via www.ccdc.cam.ac.uk/data_request/cif, or by emailing data_request@ccdc.cam.ac.uk, or by contacting The

https://doi.org/10.1021/acs.organomet.3c00493
Organometallics 2024, 43, 634−652

Cambridge Crystallographic Data Centre, 12 Union Road, Cambridge CB2 1EZ, UK; fax: + 44 1223 336033.

AUTHOR INFORMATION

Corresponding Author

Pericles Stavropoulos − *Department of Chemistry, Missouri University of Science and Technology, Rolla, Missouri 65409, United States;* orcid.org/0000-0003-0985-6203; Phone: (+1) 573-341-7220; Email: pericles@mst.edu; Fax: (+1) 573-341-6033

Authors

Meenakshi Sharma − *Department of Chemistry, Missouri University of Science and Technology, Rolla, Missouri 65409, United States;* orcid.org/0009-0003-3254-3624

Reece M. Fritz − *Department of Chemistry, Missouri University of Science and Technology, Rolla, Missouri 65409, United States*

Joseph O. Adebanjo − *Department of Chemistry, University of North Texas, Denton, Texas 76203, United States;* orcid.org/0000-0001-9877-8109

Zhou Lu − *Department of Chemistry, University of North Texas, Denton, Texas 76203, United States;* orcid.org/0000-0002-6447-4905

Thomas R. Cundari − *Department of Chemistry, University of North Texas, Denton, Texas 76203, United States;* orcid.org/0000-0003-1822-6473

Mohammad A. Omary − *Department of Chemistry, University of North Texas, Denton, Texas 76203, United States;* orcid.org/0000-0002-3247-3449

Amitava Choudhury − *Department of Chemistry, Missouri University of Science and Technology, Rolla, Missouri 65409, United States;* orcid.org/0000-0001-5496-7346

Complete contact information is available at: https://pubs.acs.org/10.1021/acs.organomet.3c00493

Funding

The authors acknowledge generous funding awarded by NIH/NIGMS (R15GM117508 and R15GM139071) for this work (to P.S.) and partial support of this research through grant DE-FG02−03ER15387 (to T.R.C.) from the U.S. Department of Energy, Basic Sciences, Catalysis Science program.

Notes

The authors declare no competing financial interest.

ACKNOWLEDGMENTS

Dr. Steven Kelley is acknowledged for collecting single-crystal X-ray diffraction data at the University of Missouri-Columbia.

REFERENCES

(1) Roose, P.; Eller, K.; Henkes, E.; Rossbacher, R.; Höke, H. Amines, Aliphatic. In *Ullmann's Encyclopedia of Industrial Chemistry*; Wiley-VCH: Wenheim, Germany, 2015.

(2) (a) Park, Y.; Kim, Y.; Chang, S. Transition Metal-Catalyzed C−H Amination: Scope, Mechanism, and Applications. *Chem. Rev.* **2017**, *117*, 9247−9301. (b) Roizen, J. L.; Harvey, M. E.; Du Bois, J. Metal-Catalyzed Nitrogen-Atom Transfer Methods for the Oxidation of Aliphatic C−H Bonds. *Acc. Chem. Res.* **2012**, *45*, 911−922. (c) Ju, M.; Schomaker, J. M. Nitrene Transfer Catalysts for Enantioselective C−N Bond Formation. *Nat. Rev. Chem.* **2021**, *5*, 580−594. (d) Chandrachud, P. P.; Jenkins, D. M. Transition Metal Aziridination Catalysts. In *Encyclopedia of Inorganic and Bioinorganic Chemistry*; Wiley Online Library, 2017; pp 1−11. (e) Cardoso, A. L.; Pinho e Melo, T. M. V. D. Aziridines in Formal [3 + 2] Cycloadditions: Synthesis of Five-Membered Heterocycles. *Eur. J. Org. Chem.* **2012**, 6479−6501.

(3) Taube, H. Observations on Atom-Transfer Reactions. In *Mechanistic Aspects of Inorganic Reactions*, Rorabacher, D. B.; Endicott, J. F., Eds.; *ACS Symposium Series*; 1982; Chapter 7, Vol. *198*, pp 151−179.

(4) (a) Mayer, J. M. Understanding Hydrogen Atom Transfer: From Bond Strengths to Marcus Theory. *Acc. Chem. Res.* **2011**, *44*, 36−46. (b) Roth, J. P.; Lovell, S.; Mayer, J. M. Intrinsic Barriers for Electron and Hydrogen Atom Transfer Reactions of Biomimetic Iron Complexes. *J. Am. Chem. Soc.* **2000**, *122*, 5486−5498. (c) Waidmann, C. R.; Zhou, X.; Tsai, E. A.; Kaminsky, W.; Hrovat, D. A.; Borden, W. T.; Mayer, J. M. Slow Hydrogen Atom Transfer Reactions of Oxo- and Hydroxo-Vanadium Compounds: The Importance of Intrinsic Barriers. *J. Am. Chem. Soc.* **2009**, *131*, 4729−4743.

(5) (a) Atienza, C. C. H.; Bowman, A. C.; Lobkovsky, E.; Chirik, P. J. Photolysis and Thermolysis of Bis(imino)pyridine Cobalt Azides: C−H Activation from Putative Cobalt Nitrido Complexes. *J. Am. Chem. Soc.* **2010**, *132*, 16343−16345. (b) Berry, J. F.; Bill, E.; Bothe, E.; DeBeer George, S.; Mienert, B.; Neese, F.; Wieghardt, K. An Octahedral Coordination Complex of Iron(VI). *Science* **2006**, *312*, 1937−1941. (c) DuBois, J.; Tomooka, C. S.; Hong, J.; Carreira, E. M. Nitridomanganese(V) Complexes: Design, Preparation, and Use as Nitrogen Atom-Transfer Reagents. *Acc. Chem. Res.* **1997**, *30*, 364−372. (d) Scepaniak, J. J.; Vogel, C. S.; Khusniyarov, M. M.; Heinemann, F. W.; Meyer, K.; Smith, J. M. Synthesis, Structure, and Reactivity of an Iron(V) Nitride. *Science* **2011**, *331*, 1049−1052. (e) Betley, T. A.; Peters, J. C. A Tetrahedrally Coordinated L_3Fe-N_x Platform that Accommodates Terminal Nitride (Fe^{IV}:N) and Dinitrogen ($Fe^{I}-N_2-Fe^{I}$) Ligands. *J. Am. Chem. Soc.* **2004**, *126*, 6252−6254.

(6) (a) Holm, R. H. Metal-centered oxygen atom transfer reactions. *Chem. Rev.* **1987**, *87*, 1401−1449. (b) Murray, L. J.; Lippard, S. J. Substrate Trafficking and Dioxygen Activation in Bacterial Multicomponent Monooxygenases. *Acc. Chem. Res.* **2007**, *40*, 466−474. (c) Cooper, H. L. R.; Mishra, G.; Huang, X.; Pendler-Cudlip, M.; Austin, R. N.; Shanklin, J.; Groves, J. T. Parallel and Competitive Pathways for Substrate Desaturation, Hydroxylation, and Radical Rearrangement by the Non-heme Diiron Hydroxylase AlkB. *J. Am. Chem. Soc.* **2012**, *134*, 20365−20375. (d) Que, L., Jr.; Tolman, W. B. Biologically inspired oxidation catalysis. *Nature* **2008**, *455*, 333−340. (e) McDonald, A. R.; Que, L., Jr High-valent nonheme iron-oxo complexes: Synthesis, structure, and spectroscopy. *Coord. Chem. Rev.* **2013**, *257*, 414−428. (f) Chen, M. S.; White, M. C. Combined Effects on Selectivity in Fe-Catalyzed Methylene Oxidation. *Science* **2010**, *327*, 566−571. (g) Nam, W.; Lee, Y.-M.; Fukuzumi, S. Tuning Reactivity and Mechanism in Oxidation Reactions by Mononuclear Nonheme Iron(IV)-Oxo Complexes. *Acc. Chem. Res.* **2014**, *47*, 1146−1154. (h) Abu-Omar, M. M. In *Physical Inorganic Chemistry, Reactions, Processes, and Applications*, Bakac, A., Ed.; John Wiley & Sons, Inc.: Hoboken, NJ, 2010; pp 75−108. (i) Peterson, R. L.; Himes, R. A.; Kotani, H.; Suenobu, T.; Tian, L.; Siegler, M.; Solomon, E. I.; Fukuzumi, S.; Karlin, K. D. Cupric Superoxo-Mediated Intermolecular C−H Activation Chemistry. *J. Am. Chem. Soc.* **2011**, *133*, 1702−1705. (j) Kundu, S.; Thompson, J. V. K.; Ryabov, A. D.; Collins, T. J. On the Reactivity of Mononuclear Iron(V)oxo Complexes. *J. Am. Chem. Soc.* **2011**, *133*, 18546−18549. (k) Taguchi, T.; Gupta, R.; Lassalle-Kaiser, B.; Boyce, D. W.; Yachandra, V. K.; Tolman, W. B.; Yano, J.; Hendrich, M. P.; Borovik, A. S. Preparation and Properties of a Monomeric High-Spin $Mn^{V}-Oxo$ Complex. *J. Am. Chem. Soc.* **2012**, *134*, 1996−1999.

(7) (a) Donahue, J. P. Thermodynamic Scales for Sulfur Atom Transfer and Oxo-for-Sulfido Exchange Reactions. *Chem. Rev.* **2006**, *106*, 4747−4783. (b) Yang, L.; Tehranchi, J.; Tolman, W. B. Reactions of Ph_3Sb = S with Copper(I) Complexes Supported by N-Donor Ligands: Formation of Stable Adducts and S-Transfer Reactivity. *Inorg. Chem.* **2011**, *50*, 2606−2612. (c) Wang, J.-J.; Kryatova, O. P.; Rybak-Akimova, E. V.; Holm, R. H. Comparative Kinetics and Mechanism of Oxygen and Sulfur Atom Transfer

Reactions Mediated by Bis(dithiolene) Complexes of Molybdenum and Tungsten. *Inorg. Chem.* **2004**, *43*, 8092−8101.
(8) (a) Matyjaszewski, K. Atom Transfer Radical Polymerization (ATRP): Current Status and Future Perspectives. *Macromolecules* **2012**, *45*, 4015−4039. (b) Pintauer, T.; Matyjaszewski, K. Atom transfer radical addition and polymerization reactions catalyzed by ppm amounts of copper complexes. *Chem. Soc. Rev.* **2008**, *37*, 1087−1097. (c) Ouchi, M.; Terashima, T.; Sawamoto, M. Transition Metal-Catalyzed Living Radical Polymerization: Toward Perfection in Catalysis and Precision Polymer Synthesis. *Chem. Rev.* **2009**, *109*, 4963−5050.
(9) (a) Hartwig, J. F. Borylation and Silylation of C−H Bonds: A Platform for Diverse C−H Bond Functionalizations. *Acc. Chem. Res.* **2012**, *45*, 864−873. (b) Mkhalid, I. A. I.; Barnard, J. H.; Marder, T. B.; Murphy, J. M.; Hartwig, J. F. C−H Activation for the Construction of C−B Bonds. *Chem. Rev.* **2010**, *110*, 890−931. (c) Obligacion, J. V.; Semproni, S. P.; Chirik, P. J. Cobalt-Catalyzed C−H Borylation. *J. Am. Chem. Soc.* **2014**, *136*, 4133−4136.
(10) (a) Doyle, M. P.; Forbes, D. C. Recent Advances in Asymmetric Catalytic Metal Carbene Transformations. *Chem. Rev.* **1998**, *98*, 911−935. (b) Davies, H. M. L.; Manning, J. R. Catalytic C−H functionalization by metal carbenoid and nitrenoid insertion. *Nature* **2008**, *451*, 417−424. (c) Davies, H. M. L.; Morton, D. Guiding principles for site selective and stereoselective intermolecular C−H functionalization by donor/acceptor rhodium carbenes. *Chem. Soc. Rev.* **2011**, *40*, 1857−1869. (d) Deng, Y.; Qiu, H.; Srinivas, H. D.; Doyle, M. P. Chiral Dirhodium(II) Catalysts for Selective Metal Carbene Reactions. *Curr. Org. Chem.* **2016**, *20*, 61−81. (e) Ford, A.; Miel, H.; Ring, A.; Slattery, C. N.; Maguire, A. R.; McKervey, M. A. Modern Organic Synthesis with α-Diazocarbonyl Compounds. *Chem. Rev.* **2015**, *115*, 9981−10080. (f) Ebner, C.; Carreira, E. M. Cyclopropanation Strategies in Recent Total Syntheses. *Chem. Rev.* **2017**, *117*, 11651−11679. (i) Wang, B.; Qiu, D.; Zhang, Y.; Wang, J. Recent advances in C(sp^3)−H bond functionalization via metal−carbene insertions. *Beilstein J. Org. Chem.* **2016**, *12*, 796−804.
(11) (a) Zalatan, D. N.; Du Bois, J. Metal-Catalyzed Oxidations of C−H to C−N Bonds. *Top. Curr. Chem.* **2010**, *292*, 347−378. (b) Roizen, J. L.; Harvey, M. E.; Du Bois, J. Metal-Catalyzed Nitrogen-Atom Transfer Methods for the Oxidation of Aliphatic C−H Bonds. *Acc. Chem. Res.* **2012**, *45*, 911−922. (c) Gephart, R. T., III; Warren, T. H. Copper-Catalyzed sp^3 C−H Amination. *Organometallics* **2012**, *31*, 7728−7752. (d) Collet, F.; Lescot, C.; Dauban, P. Catalytic C−H amination: the stereoselectivity issue. *Chem. Soc. Rev.* **2011**, *40*, 1926−1936. (e) Dequirez, G.; Pons, V.; Dauban, P. Nitrene Chemistry in Organic Synthesis: Still in Its Infancy? *Angew. Chem., Int. Ed.* **2012**, *51*, 7384−7395. (f) Hazelard, D.; Nocquet, P.-A.; Compain, P. Catalytic C−H amination at its limits: challenges and solutions. *Org. Chem. Front.* **2017**, *4*, 2500−2521. (g) Uchida, T.; Katsuki, T. Asymmetric Nitrene Transfer Reactions: Sulfimidation, Aziridination and C−H Amination Using Azide Compounds as Nitrene Precursors. *Chem. Rec.* **2014**, *14*, 117−129. (h) Pellissier, H. Recent Developments in Asymmetric Aziridination. *Adv. Synth. Catal.* **2014**, *356*, 1899−1935. (i) Díaz-Requejo, M. M.; Pérez, P. J. Coinage Metal Catalyzed C−H Bond Functionalization of Hydrocarbons. *Chem. Rev.* **2008**, *108*, 3379−3394. (j) Müller, P.; Fruit, C. Enantioselective Catalytic Aziridinations and Asymmetric Nitrene Insertions into CH Bonds. *Chem. Rev.* **2003**, *103*, 2905−2919.
(12) (a) Huang, X.; Bergsten, T. V.; Groves, J. T. Manganese-Catalyzed Late-Stage Aliphatic C−H Azidation. *J. Am. Chem. Soc.* **2015**, *137*, 5300−5303. (b) Sharma, A.; Hartwig, J. F. Metal-catalysed azidation of tertiary C−H bonds suitable for late−stage functionalization. *Nature* **2015**, *517*, 600−604. (c) Karimov, R. R.; Sharma, A.; Hartwig, J. F. Late Stage Azidation of Complex Molecules. *ACS Cent. Sci.* **2016**, *2*, 715−724.
(13) (a) Coin, G.; Latour, J.-M. Nitrene transfers mediated by natural and artificial iron enzymes. *J. Inorg. Biochem.* **2021**, *225*, 111613. (b) Bollinger, J. M.; Broderick, J. B. Frontiers in enzymatic C−H-bond activation. *Curr. Opin. Chem. Biol.* **2009**, *13*, 51−57. (c) Lewis, J. C.; Coelho, P. S.; Arnold, F. H. Enzymatic functionalization of carbon−hydrogen bonds. *Chem. Soc. Rev.* **2011**, *40*, 2003−2021. (d) Yang, Y.; Arnold, F. H. Navigating the Unnatural Reaction Space: Directed Evolution of Heme Proteins for Selective Carbene and Nitrene Transfer. *Acc. Chem. Res.* **2021**, *54*, 1209−1225. (e) Brandenberg, O. F.; Fasan, R.; Arnold, F. H. Exploiting and engineering hemoproteins for abiological carbene and nitrene transfer reactions. *Curr. Opin. Biotechnol.* **2017**, *47*, 102−111.
(14) Hartwig, J. F.; Larsen, M. A. Undirected, Homogeneous C−H Bond Functionalization: Challenges and Opportunities. *ACS Cent. Sci.* **2016**, *2*, 281−292.
(15) (a) Combee, L. A.; Raya, B.; Wang, D.; Hilinski, M. K. Organocatalytic nitrenoid transfer: metal-free selective intermolecular C(sp^3)−H amination catalyzed by an iminium salt. *Chem. Sci.* **2018**, *9*, 935−939. (b) Qin, Q.; Yu, S. Visible-Light-Promoted Remote C(sp^3)−H Amidation and Chlorination. *Org. Lett.* **2015**, *17*, 1894−1897. (c) Pandey, G.; Laha, R. Visible-Light-Catalyzed Direct Benzylic C(sp^3)−H Amination Reaction by Cross-Dehydrogenative Coupling. *Angew. Chem., Int. Ed.* **2015**, *54*, 14875−14879. (d) Zhu, C.; Liang, Y.; Hong, X.; Sun, H.; Sun, W.-Y.; Houk, K. N.; Shi, Z. Iodoarene-Catalyzed Stereospecific Intramolecular sp^3 C−H Amination: Reaction Development and Mechanistic Insights. *J. Am. Chem. Soc.* **2015**, *137*, 7564−7567. (e) Souto, J. A.; Martínez, C.; Velilla, I.; Muñiz, K. Defined Hypervalent Iodine(III) Reagents Incorporating Transferrable Nitrogen Groups: Nucleophilic Amination through Electrophilic Activation. *Angew. Chem. Int. Ed.* **2013**, *52*, 1324−1328. (f) Souto, J. A.; Zian, D.; Muñiz, K. Iodine(III)-Mediated Intermolecular Allylic Amination under Metal-Free Conditions. *J. Am. Chem. Soc.* **2012**, *134*, 7242−7245. (g) Kim, H. J.; Kim, J.; Cho, S. H.; Chang, S. Intermolecular Oxidative C−N Bond Formation under Metal-Free Conditions: Control of Chemoselectivity between Aryl sp^2 and Benzylic sp^3 C−H Bond Imidation. *J. Am. Chem. Soc.* **2011**, *133*, 16382−16385. (h) Kantak, A. A.; Potavathri, S.; Barham, R. A.; Romano, K. M.; DeBoef, B. Metal-Free Intermolecular Oxidative C−N Bond Formation via Tandem C−H and N−H Bond Functionalization. *J. Am. Chem. Soc.* **2011**, *133*, 19960−19965. (i) Antonchick, A. P.; Samanta, R.; Kulikov, K.; Lategahn, J. Organocatalytic, Oxidative, Intramolecular C−H Bond Amination and Metal-free Cross-Amination of Unactivated Arenes at Ambient Temperature. *Angew. Chem., Int. Ed.* **2011**, *50*, 8605−8608. (j) Ochiai, M.; Miyamoto, K.; Kaneaki, T.; Hayashi, S.; Nakanishi, W. Highly Regioselective Amination of Unactivated Alkanes by Hypervalent Sulfonylimino-λ^3-Bromane. *Science* **2011**, *332*, 448−451.
(16) (a) Chu, J. C. K.; Rovis, T. Complementary Strategies for Directed C(sp^3)−H Functionalization: A Comparison of Transition-Metal-Catalyzed Activation, Hydrogen Atom Transfer, and Carbene/Nitrene Transfer. *Angew. Chem., Int. Ed.* **2018**, *57*, 62−101.
(17) Selective examples of typical Rh-centered C−N Bond Formation: (a) Fiori, K. W.; Du Bois, J. Catalytic Intermolecular Amination of C−H Bonds: Method Development and Mechanistic Insights. *J. Am. Chem. Soc.* **2007**, *129*, 562−568. (b) Fiori, K. W.; Espino, C. G.; Brodsky, B. H.; Du Bois, J. A mechanistic analysis of the Rh-catalyzed intramolecular C−H amination reaction. *Tetrahedron* **2009**, *65*, 3042−3051. (c) Zalatan, D. N.; Du Bois, J. Understanding the Differential Performance of $Rh_2(esp)_2$ as a Catalyst for C−H Amination. *J. Am. Chem. Soc.* **2009**, *131*, 7558−7559. (d) Liang, C.; Collet, F.; Robert-Peillard, F.; Müller, P.; Dodd, R. H.; Dauban, P. Toward a Synthetically Useful Stereoselective C−H Amination of Hydrocarbons. *J. Am. Chem. Soc.* **2008**, *130*, 343−350. (e) Liang, C.; Robert-Peillard, F.; Fruit, C.; Müller, P.; Dodd, R. H.; Dauban, P. Efficient Diastereoselective Intermolecular Rhodium-Catalyzed C-H Amination. *Angew. Chem., Int. Ed.* **2006**, *45*, 4641−4644. (f) Nägeli, I.; Baud, C.; Bernardinelli, G.; Jacquier, Y.; Moran, M.; Müller, P. Rhodium(II)-Catalyzed CH Insertions with {[(4-Nitrophenyl)-sulfonyl]imino}phenyl-λ^3-iodane. *Helv. Chim. Acta* **1997**, *80*, 1087−1105. (g) Huard, K.; Lebel, H. N-Tosyloxycarbamates as Reagents in Rhodium-Catalyzed C−H Amination Reactions. *Chem.—Eur. J.* **2008**, *14*, 6222−6230. (h) Lebel, H.; Huard, K.; Lectard, S. N-Tosyloxycarbamates as a Source of Metal Nitrenes: Rhodium-Catalyzed C−H Insertion and Aziridination Reactions. *J.*

https://doi.org/10.1021/acs.organomet.3c00493
Organometallics 2024, 43, 634−652

Am. Chem. Soc. **2005**, *127*, 14198−14199. (i) Reddy, R. P.; Davies, H. M. L. Dirhodium Tetracarboxylates Derived from Adamantylglycine as Chiral Catalysts for Enantioselective C−H Aminations. *Org. Lett.* **2006**, *8*, 5013−5016. (j) Nguyen, Q.; Sun, K.; Driver, T. G. Rh_2(II)-Catalyzed Intramolecular Aliphatic C−H Bond Amination Reactions Using Aryl Azides as the N-Atom Source. *J. Am. Chem. Soc.* **2012**, *134*, 7262−7265. (k) Jat, J. L.; Paudyal, M. P.; Gao, H.; Xu, Q.-L.; Yousufuddin, M.; Devarajan, D.; Ess, D. H.; Kürti, L.; Falck, J. R. Direct Stereospecific Synthesis of Unprotected N-H and N-Me Aziridines from Olefins. *Science* **2014**, *343*, 61−65. (l) Ma, Z.; Zhou, Z.; Kürti, L. Direct and Stereospecific Synthesis of *N*-H and *N*-Alkyl Aziridines from Unactivated Olefins Using Hydroxylamine-*O*-Sulfonic Acids. *Angew. Chem., Int. Ed.* **2017**, *56*, 9886−9890.

(18) Selective examples of typical Cu-centered C−N Bond Formation: (a) Aguila, M. J. B.; Badiei, Y. M.; Warren, T. H. Mechanistic Insights into C−H Amination via Dicopper Nitrenes. *J. Am. Chem. Soc.* **2013**, *135*, 9399−9406. (b) Badiei, Y. M.; Dinescu, A.; Dai, X.; Palomino, R. M.; Heinemann, F. W.; Cundari, T. R.; Warren, T. H. Copper−Nitrene Complexes in Catalytic C−H Amination. *Angew. Chem., Int. Ed.* **2008**, *47*, 9961−9964. (c) Barman, D. N.; Liu, P.; Houk, K. N.; Nicholas, K. M. On the Mechanism of Ligand-Assisted, Copper-Catalyzed Benzylic Amination by Chloramine-T. *Organometallics* **2010**, *29*, 3404−3412. (d) Barman, D.; Nicholas, K. M. Ligand-assisted, copper-catalyzed enantioselective benzylic amination. *Tetrahedron Lett.* **2010**, *51*, 1815−1818. (e) Fructos, M. R.; Trofimenko, S.; Díaz-Requejo, M. M.; Pérez, P. J. Facile Amine Formation by Intermolecular Catalytic Amidation of Carbon−Hydrogen Bonds. *J. Am. Chem. Soc.* **2006**, *128*, 11784−11791. (f) Gómez-Emeterio, B. P.; Urbano, J.; Díaz-Requejo, M. M.; Pérez, P. J. Easy Alkane Catalytic Functionalization. *Organometallics* **2008**, *27*, 4126−4130. (g) Díaz-Requejo, M. M.; Pérez, P. J.; Brookhart, M.; Templeton, J. L. Substituent Effects on the Reaction Rates of Copper-Catalyzed Cyclopropanation and Aziridination of para-Substituted Styrenes. *Organometallics* **1997**, *16*, 4399−4402. (h) Lebel, H.; Parmentier, M. Copper-catalyzed enantioselective aziridination of styrenes. *Pure Appl. Chem.* **2010**, *82*, 1827−1833. (i) Lebel, H.; Lectard, S.; Parmentier, M. Copper-Catalyzed Alkene Aziridination with N-Tosyloxycarbamates. *Org. Lett.* **2007**, *9*, 4797−4800. (j) Powell, D. A.; Fan, H. Copper-Catalyzed Amination of Primary Benzylic C−H Bonds with Primary and Secondary Sulfonamides. *J. Org. Chem.* **2010**, *75*, 2726−2729. (k) Pelletier, G.; Powell, D. A. Copper-Catalyzed Amidation of Allylic and Benzylic C-H Bonds. *Org. Lett.* **2006**, *8*, 6031−6034. (l) Comba, P.; Haaf, C.; Lienke, A.; Muruganantham, A.; Wadepohl, H. Synthesis, Structure, and Highly Efficient Copper-Catalyzed Aziridination with a Tetraaza-Bispidine Ligand. *Chem.—Eur. J.* **2009**, *15*, 10880−10887. (m) Vedernikov, A. N.; Caulton, K. G. Facile alkane functionalization in copper-[2.1.1]-(2,6)-pyridinophane-PhINTs systems. *Chem. Commun.* **2004**, 162−163. (n) Evans, D. A.; Faul, M. M.; Bilodeau, M. T. Development of the Copper-Catalyzed Olefin Aziridination Reaction. *J. Am. Chem. Soc.* **1994**, *116*, 2742−2753. (o) Li, Z.; Quan, R. W.; Jacobsen, E. N. Mechanism of the (Diimine)copper-Catalyzed Asymmetric Aziridination of Alkenes. Nitrene Transfer via Ligand-Accelerated Catalysis. *J. Am. Chem. Soc.* **1995**, *117*, 5889−5890.

(19) (a) Paraskevopoulou, P.; Lin, A.; Wang, Q.; Pinnapareddy, D.; Acharrya, R.; Dinda, R.; Çelenligil-Çetin, R.; Floros, G.; Sanakis, Y.; Choudhury, A.; Rath, N. P.; Stavropoulos, P. Synthesis and Characterization of a Series of Structurally and Electronically Diverse Fe(II) Complexes Featuring a Family of Triphenylamido-amine Ligands. *Inorg. Chem.* **2010**, *49*, 108−122. (b) Çelenligil-Çetin, R.; Paraskevopoulou, P.; Dinda, R.; Staples, R. J.; Sinn, E.; Rath, N. P.; Stavropoulos, P. Synthesis, Characterization, and Reactivity of Iron Trisamidoamine Complexes that Undergo both Metal- and Ligand-Centered Oxidative Transformations. *Inorg. Chem.* **2008**, *47*, 1165−1172. (c) Çelenligil-Çetin, R.; Paraskevopoulou, P.; Lalioti, N.; Sanakis, Y.; Staples, R. J.; Rath, N. P.; Stavropoulos, P. Metalloradical Complexes of Manganese and Chromium Featuring an Oxidatively Rearranged Ligand. *Inorg. Chem.* **2008**, *47*, 10998−11009. (d) Çelenligil-Çetin, R.; Paraskevopoulou, P.; Dinda, R.; Lalioti, N.; Sanakis, Y.; Rawashdeh, A. M.; Staples, R. J.; Sinn, E.; Stavropoulos, P. Oxidative Ligand Rearrangement due to Incipient Aminyl Radicals in the Oxidation of Iron(II) Species with Dioxygen. *Eur. J. Inorg. Chem.* **2008**, *2008*, 673−677.

(20) (a) Schrock, R. R. Transition Metal Complexes that Contain a Triamidoamine Ligand. *Acc. Chem. Res.* **1997**, *30*, 9−16. (b) Verkade, J. G. Atranes: New Examples with Unexpected Properties. *Acc. Chem. Res.* **1993**, *26*, 483−489.

(21) (a) Borovik, A. S. Bio-Inspired Hydrogen Bond Motifs in Ligand Design: The Role of Noncovalent Interactions in Metal Ion Mediated Activation of Dioxygen. *Acc. Chem. Res.* **2005**, *38*, 54−61. (b) Gupta, R.; Borovik, A. S. Monomeric $Mn^{III/II}$ and $Fe^{III/II}$ Complexes with Terminal Hydroxo and Oxo Ligands: Probing Reactivity via O−H Bond Dissociation Energies. *J. Am. Chem. Soc.* **2003**, *125*, 13234−13242. (c) MacBeth, C. E.; Golombek, A. P.; Young, V. G., Jr.; Yang, C.; Kuczera, K.; Hendrich, M. P.; Borovik, A. S. O_2 Activation by Nonheme Iron Complexes: A Monomeric Fe(III)−Oxo Complex Derived From O_2. *Science* **2000**, *289*, 938−941.

(22) (a) Freundlich, J. S.; Schrock, R. R.; Davis, W. M. Synthetic and Mechanistic Investigations of Trimethylsilyl-Substituted Triamidoamine Complexes of Tantalum That Contain Metal-Ligand Multiple Bonds. *J. Am. Chem. Soc.* **1996**, *118*, 3643−3655. (b) Yandulov, D. V.; Schrock, R. R. Catalytic Reduction of Dinitrogen to Ammonia at a Single Molybdenum Center. *Science* **2003**, *301*, 76−78. (c) Yandulov, D. V.; Schrock, R. R. Reduction of Dinitrogen to Ammonia at a Well-Protected Reaction Site in a Molybdenum Triamidoamine Complex. *J. Am. Chem. Soc.* **2002**, *124*, 6252−6253. (d) Greco, G. E.; Schrock, R. R. Synthesis of Triamidoamine Ligands of the Type $(ArylNHCH_2CH_2)_3N$ and Molybdenum and Tungsten Complexes That Contain an $[(ArylNCH_2CH_2)_3N]^{3-}$ Ligand. *Inorg. Chem.* **2001**, *40*, 3850−3860. (e) Greco, G. E.; Schrock, R. R. Synthesis, Structure, and Electrochemical Studies of Molybdenum and Tungsten Dinitrogen, Diazenido, and Hydrazido Complexes that Contain Aryl-Substituted Triamidoamine Ligands. *Inorg. Chem.* **2001**, *40*, 3861−3878. (f) Cummins, C. C.; Schrock, R. R. Synthesis of an Iron(IV) Cyanide Complex that Contains the Triamido Amine Ligand $[(t\text{-}BuMe_2SiNCH_2CH_2)_3N]^{3-}$. *Inorg. Chem.* **1994**, *33*, 395−396.

(23) (a) Villanueva, O.; Weldy, N. M.; Blakey, S. B.; MacBeth, C. E. Cobalt catalyzed sp^3 C−H amination utilizing aryl azides. *Chem. Sci.* **2015**, *6*, 6672−6675. (b) Corcos, A. R.; Villanueva, O.; Walroth, R. C.; Sharma, S. K.; Basca, J.; Lancaster, K. M.; MacBeth, C. E.; Berry, J. F. Oxygen Activation by Co(II) and a Redox Non-Innocent Ligand: Spectroscopic Characterization of a Radical−Co(II)−Superoxide Complex with Divergent Catalytic Reactivity. *J. Am. Chem. Soc.* **2016**, *138*, 1796−1799. (c) Krogman, J. P.; Thomas, C. M. Metal-metal multiple bonding in C_3-symmetric bimetallic complexes of the first row transition metals. *Chem. Commun.* **2014**, *50*, 5115−5127. (d) Cammarota, R. C.; Vollmer, M. V.; Xie, J.; Ye, J.; Linehan, J. C.; Burgess, S. A.; Appel, A. M.; Gagliardi, L.; Lu, C. C. A Bimetallic Nickel−Gallium Complex Catalyzes CO_2 Hydrogenation via the Intermediacy of an Anionic d^{10} Nickel Hydride. *J. Am. Chem. Soc.* **2017**, *139*, 14244−14250.

(24) (a) Kalra, A.; Bagchi, V.; Paraskevopoulou, P.; Das, P.; Ai, L.; Sanakis, Y.; Raptopoulos, G.; Mohapatra, S.; Choudhury, A.; Sun, Z.; Cundari, T. R.; Stavropoulos, P. Is the Electrophilicity of the Metal Nitrene the Sole Predictor of Metal-Mediated Nitrene Transfer to Olefins? Secondary Contributing Factors as Revealed by a Library of High-Spin Co(II) Reagents. *Organometallics* **2021**, *40*, 1974−1996. (b) Bagchi, V.; Kalra, A.; Das, P.; Paraskevopoulou, P.; Gorla, S.; Ai, L.; Wang, Q.; Mohapatra, S.; Choudhury, A.; Sun, Z.; Cundari, T. R.; Stavropoulos, P. Comparative Nitrene-Transfer Chemistry to Olefinic Substrates Mediated by a Library of Anionic Mn(II) Triphenylamido-Amine Reagents and M(II) Congeners (M = Fe, Co, Ni) Favoring Aromatic over Aliphatic Alkenes. *ACS Catal.* **2018**, *8*, 9183−9206.

(25) (a) Wittman, H.; Raab, V.; Schorm, A.; Plackmeyer, J.; Sundermeyer, J. Complexes of Manganese, Iron, Zinc, and Molybdenum with a Superbasic Tris(guanidine) Derivative of

https://doi.org/10.1021/acs.organomet.3c00493
Organometallics 2024, 43, 634−652

Tris(2-ethylamino)amine (Tren) as a Tripod Ligand. *Eur. J. Inorg. Chem.* **2001**, 1937−1948. (b) Stanek, J.; Rösener, T.; Metz, A.; Mannsperger, J.; Hoffmann, A.; Herres-Pawlis, S. Guanidine Metal Complexes for Bioinorganic Chemistry and Polymerisation Catalysis. *Top. Heterocycl. Chem.* **2015**, *51*, 95−164. (c) Bienemann, O.; Hoffman, A.; Herres-Pawlis, S. (Guanidine)copper complexes: structural variety and applications in bioinorganic chemistry and catalysis. *Rev. Inorg. Chem.* **2011**, *31*, 83−108. (d) Cui, X.-Y.; Tan, C.-H.; Leow, D. Metal-catalysed reactions enabled by guanidine-type ligands. *Org. Biomol. Chem.* **2019**, *17*, 4689−4699.

(26) (a) Malik, D. D.; Chandra, A.; Seo, M. S.; Lee, Y.-M.; Farquhar, E. R.; Mebs, S.; Dau, H.; Ray, K.; Nam, W. Formation of cobalt-oxygen intermediates by dioxygen activation at a mononuclear nonheme cobalt(II) center. *Dalton Trans.* **2021**, *50*, 11889−11898. (b) Comba, P.; Löhr, A.-M.; Pfaff, F.; Ray, K. Redox Potentials of High-Valent Iron-, Cobalt-, and Nickel-Oxido Complexes: Evidence for Exchange Enhanced Reactivity. *Isr. J. Chem.* **2020**, *60*, 957−962. (c) Liu, J. J.; Siegler, M. A.; Karlin, K. D.; Moënne-Loccoz, P. Direct Resonance Raman Characterization of a Peroxynitrito Copper Complex Generated from O_2 and NO and Mechanistic Insights into Metal-Mediated Peroxynitrite Decomposition. *Angew. Chem., Int. Ed.* **2019**, *58*, 10936−10940. (d) Speelman, A. L.; White, C. J.; Zhang, B.; Alp, E. E.; Zhao, J.; Hu, M.; Krebs, C.; Penner-Hahn, J.; Lehnert, N. Non-heme High-Spin $\{FeNO\}^{6-8}$ Complexes: One Ligand Platform Can Do it All. *J. Am. Chem. Soc.* **2018**, *140*, 11341−11359. (e) Saracini, C.; Liakos, D. G.; Rivera, J. E. Z.; Neese, F.; Meyer, G. J.; Karlin, K. D. Excitation Wavelength Dependent O_2 Release from Copper(II)−Superoxide Compounds: Laser Flash-Photolysis Experiments and Theoretical Studies. *J. Am. Chem. Soc.* **2014**, *136*, 1260−1263. (f) Peterson, R. L.; Ginsbach, J. W.; Cowley, R. E.; Qayyum, M. F.; Himes, R. A.; Siegler, M. A.; Moore, C. D.; Hedman, B.; Hodgson, K. O.; Fukuzumi, S.; Solomon, E. I.; Karlin, K. D. Stepwise Protonation and Electron-Transfer Reduction of a Primary Copper−Dioxygen Adduct. *J. Am. Chem. Soc.* **2013**, *135*, 16454−16467. (g) Pfaff, F. F.; Kundu, S.; Risch, M.; Pandian, S.; Heims, F.; Pryjomska-Ray, I.; Haack, P.; Metzinger, R.; Bill, E.; Dau, H.; Comba, P.; Ray, K. An Oxocobalt(IV) Complex Stabilized by Lewis Acid Interactions with Scandium(III) Ions. *Angew. Chem., Int. Ed.* **2011**, *50*, 1711−1715. (h) England, J.; Guo, Y.; Van Heuvelen, K. M.; Cranswick, M. A.; Rohde, G. T.; Bominaar, E. L.; Münck, E.; Que, L., Jr. A More Reactive Trigonal-Bipyramidal High-Spin Oxoiron(IV) Complex with a cis-Labile Site. *J. Am. Chem. Soc.* **2011**, *133*, 11880−11883.

(27) Bagchi, V.; Paraskevopoulou, P.; Das, P.; Chi, L.; Wang, Q.; Choudhury, A.; Mathieson, J. S.; Cronin, L.; Pardue, D. B.; Cundari, T. R.; Mitrikas, G.; Sanakis, Y.; Stavropoulos, P. A versatile Tripodal Cu(I) Reagent for C−N Bond Construction via Nitrene-Transfer Chemistry: Catalytic Perspectives and Mechanistic Insights on C−H Aminations/Amidinations and Olefin Aziridinations. *J. Am. Chem. Soc.* **2014**, *136*, 11362−11381.

(28) Sahoo, S. K.; Harfmann, B.; Ai, L.; Wang, Q.; Mohapatra, S.; Choudhury, A.; Stavropoulos, P. Cationic Divalent Metal Sites (M = Mn, Fe, Co) Operating as Both Nitrene-Transfer Agents and Lewis Acids toward Mediating the Synthesis of Three- and Five-Membered *N*-Heterocycles. *Inorg. Chem.* **2023**, *62*, 10743−10761.

(29) You, D.; Gabbaï, F. P. Tunable σ-Accepting, Z-Type Ligands for Organometallic Catalysis. *Trends Chem.* **2019**, *1*, 485−496.

(30) Bernasconi, L.; Louwerse, M. J.; Baerends, E. J. The Role of Equatorial and Axial Ligands in Promoting the Activity of Non-Heme Oxidoiron(IV) Catalysts in Alkane Hydroxylation. *Eur. J. Inorg. Chem.* **2007**, *2007*, 3023−3033.

(31) Liang, H.-C.; Kim, E.; Incarvito, C. D.; Rheingold, A. L.; Karlin, K. D. A Bis-Acetonitrile Two-Coordinate Copper(I) Complex: Synthesis and Characterization of Highly Soluble $B(C_6F_5)_4^-$ Salts of $[Cu(MeCN)_2]^+$ and $[Cu(MeCN)_4]^+$. *Inorg. Chem.* **2002**, *41*, 2209−2212.

(32) (a) Sletten, E. T.; Tu, Y.-J.; Schlegel, H. B.; Nguyen, H. M. Are Brønsted Acids the True Promoter of Metal-Triflate-Catalyzed Glycosylations? A Mechanistic Probe into 1,2-*cis*-Aminoglycoside Formation by Nickel Triflate. *ACS Catal.* **2019**, *9*, 2110−2123. (b) Chen, J.; Goforth, S. K.; McKeown, B. A.; Gunnoe, T. B. Brønsted acid-catalysed intramolecular hydroamination of unactivated alkenes: metal triflates as an *in situ* source of triflic acid. *Dalton Trans.* **2017**, *46*, 2884−2891. (c) Tschan, M. J.-L.; Thomas, C. M.; Strub, H.; Carpentier, J.-F. Copper(II) Triflate as a Source of Triflic Acid: Effective, Green Catalysis of Hydroalkoxylation Reactions. *Adv. Synth. Catal.* **2009**, *351*, 2496−2504. (d) Rosenfeld, D. C.; Shekhar, S.; Takemiya, A.; Utsunomiya, M.; Hartwig, J. F. Hydroamination and Hydroalkoxylation Catalyzed by Triflic Acid. Parallels to Reactions Initiated with Metal Triflates. *Org. Lett.* **2006**, *8*, 4179−4182. (e) Dumeunier, R.; Markó, I. E. On the role of triflic acid in the metal triflate-catalysed acylation of alcohols. *Tetrahedron Lett.* **2004**, *45*, 825−829.

(33) Ke, I.-S.; Gabbaï, F. P. $Cu_3(\mu_2\text{-}Cl)_3$ and $Ag_3(\mu_2\text{-}Cl)_3$ Complexes Supported by Tetradentate Trisphosphino-stibine and -bismuthine Ligands: Structural Evidence for Triply Bridging Heavy Pnictines. *Aust. J. Chem.* **2013**, *66*, 1281−1287.

(34) Baranov, A. Y.; Pritchina, E. A.; Berezin, A. S.; Samsonenko, D. G.; Fedin, V. P.; Belogorlova, N. A.; Gritsan, N. P.; Artem′ev, A. V. Beyond Classical Coordination Chemistry: The First Case of a Triply Bridging Phosphine Ligand. *Angew. Chem., Int. Ed.* **2021**, *60*, 12577−12584.

(35) Hargittai, M.; Schwerdtfeger, P.; Réffy, B.; Brown, R. The Molecular Structure of Different Species of Cuprous Chloride from Gas-Phase Electron Diffraction and Quantum Chemical Calculations. *Chem.—Eur. J.* **2003**, *9*, 327−333.

(36) Cordero, B.; Gómez, V.; Platero-Prats, A. E.; Revés, M.; Echeverría, J.; Cremades, E.; Barragán, F.; Alvarez, S. Covalent radii revisited. *Dalton Trans.* **2008**, 2832−2838.

(37) (a) Zhang, L.; Li, X.-X.; Lang, Z.-L.; Liu, Y.; Liu, J.; Yuan, L.; Lu, W.-Y.; Xia, Y.-S.; Dong, L.-Z.; Yuan, D.-Q.; Lan, Y.-Q. Enhanced Cuprophilic Interactions in Crystalline Catalysts Facilitate the Highly Selective Electroreduction of CO_2 to CH_4. *J. Am. Chem. Soc.* **2021**, *143*, 3808−3816. (b) Harisomayajula, N. V. S.; Makovetskyi, S.; Tsai, Y.-C. Cuprophilic Interactions in and between Molecular Entities. *Chem. - Eur. J.* **2019**, *25*, 8936−8954. (c) Singh, K.; Long, J. R.; Stavropoulos, P. Ligand-Unsupported Metal−Metal (M = Cu, Ag) Interactions between Closed-Shell d^{10} Trinuclear Systems. *J. Am. Chem. Soc.* **1997**, *119*, 2942−2943.

(38) Alvarez, S. A cartography of the van der Waals territories. *Dalton Trans.* **2013**, *42*, 8617−8636.

(39) Yang, L.; Powell, D. R.; Houser, R. P. Structural variation in copper(I) complexes with pyridylmethylamide ligands: structural analysis with a new four-coordinate geometry index, τ_4. *Dalton Trans.* **2007**, 955−964.

(40) Mantina, M.; Chamberlin, A. C.; Valero, R.; Cramer, C. J.; Truhlar, D. G. Consistent van der Waals Radii for the Whole Main Group. *J. Phys. Chem. A* **2009**, *113*, 5806−5812.

(41) García-Romero, Á.; Waters, J. E.; Jethwa, R. B.; Bond, A. D.; Colebatch, A. L.; García-Rodríguez, R.; Wright, D. S. *Inorg. Chem.* **2023**, *62*, 4625−4636.

(42) Taylor, W. V.; Cammack, C. X.; Shubert, S. A.; Rose, M. J. Thermoluminescent Antimony-Supported Copper-Iodo Cuboids: Approaching NIR Emission via High Crystallographic Symmetry. *Inorg. Chem.* **2019**, *58*, 16330−16345.

(43) (a) Mitoraj, M. P.; Michalak, A.; Ziegler, T. A Combined Charge and Energy Decomposition Scheme for Bond Analysis. *J. Chem. Theory Comput.* **2009**, *5*, 962−975. (b) Ziegler, T.; Rauk, A. Carbon Monoxide, Carbon Monosulfide, Molecular Nitrogen, Phosphorus Trifluoride, and Methyl Isocyanide as σ Donors and π Acceptors. A Theoretical Study by the Hartree-Fock-Slater Transition-State Method. *Inorg. Chem.* **1979**, *18*, 1755−1759. (c) Ziegler, T.; Rauk, A. A Theoretical Study of the Ethylene-Metal Bond in Complexes between Cu^+, Ag^+, Au^+, Pt^0 or Pt^{2+} and Ethylene, Based on the Hartree-Fock-Slater Transition-State Method. *Inorg. Chem.* **1979**, *18*, 1558−1565.

https://doi.org/10.1021/acs.organomet.3c00493
Organometallics 2024, 43, 634−652

(44) Lu, T.; Chen, Q. Independent gradient model based on Hirshfeld partition: A new method for visual study of interactions in chemical systems. *J. Comput. Chem.* **2022**, *43*, 539−555.
(45) Greenacre, V. K.; Levason, W.; Reid, G. Developments in the chemistry of stibine and bismuthine complexes. *Coord. Chem. Rev.* **2021**, *432*, 213698.
(46) Al-Ajlouni, A.; Espenson, J. H. Epoxidation of Styrenes by Hydrogen Peroxide As Catalyzed by Methylrhenium Trioxide. *J. Am. Chem. Soc.* **1995**, *117*, 9243−9250.
(47) Müller, P.; Baud, C.; Jacquier, Y.; Moran, M.; Nägeli, I. Rhodium(II)-Catalyzed Aziridinations and CH Insertions with [*N*-(*p*-Nitrobenzenesulfonyl)Imino]Phenyliodinane. *J. Phys. Org. Chem.* **1996**, *9*, 341−347.
(48) Neuenschwander, U.; Hermans, I. The Conformations of Cyclooctene: Consequences for Epoxidation Chemistry. *J. Org. Chem.* **2011**, *76*, 10236−10240.
(49) Van Leest, N. P.; Grooten, L.; van der Vlugt, J. I.; de Bruin, B. Uncatalyzed Oxidative C−H Amination of 9,10-Dihydro-9-Hetero-anthracenes: A Mechanistic Study. *Chem.—Eur. J.* **2019**, *25*, 5987−5993.
(50) Nam, P.-C.; Nguyen, M. T.; Chandra, A. K. The C−H and α(C−X) Bond Dissociation Enthalpies of Toluene, C_6H_5-CH_2X (X = F, Cl), and Their Substituted Derivatives: A DFT Study. *J. Phys. Chem. A* **2005**, *109*, 10342−10347.
(51) Rodríguez, M. R.; Rodríguez, A. M.; López-Resano, S.; Pericàs, M. A.; Díaz-Requejo, M. M.; Maseras, F.; Pérez, P. J. Non-innocent Role of the Halide Ligand in the Copper-Catalyzed Olefin Aziridination Reaction. *ACS Catal.* **2023**, *13*, 706−713.
(52) Harvey, M. E.; Musaev, D.; Du Bois, J. A Diruthenium Catalyst for Selective, Intramolecular Allylic C−H Amination: Reaction Development and Mechanistic Insight Gained through Experiment and Theory. *J. Am. Chem. Soc.* **2011**, *133*, 17207−17216.
(53) Park, S. H.; Kwak, J.; Shin, K.; Ryu, J.; Park, Y.; Chang, S. Mechanistic Studies of the Rhodium-Catalyzed Direct C−H Amination Reaction Using Azides as the Nitrogen Source. *J. Am. Chem. Soc.* **2014**, *136*, 2492−2502.
(54) (a) Wächtler, E.; Gericke, R.; Block, T.; Pöttgen, R.; Wagler, J. Trivalent Antimony as L-, X-, and Z-Type Ligand: The Full Set of Possible Coordination Modes in Pt−Sb Bonds. *Inorg. Chem.* **2020**, *59*, 15541−15552. (b) Benjamin, S. L.; Krämer, T.; Levason, W.; Light, M. E.; Macgregor, S. A.; Reid, G. $[Pd_4(\mu_3\text{-}SbMe_3)_4(SbMe_3)_4]$: A Pd(0) Tetrahedron with μ_3-Bridging Trimethylantimony Ligands. *J. Am. Chem. Soc.* **2016**, *138*, 6964−6967.
(55) (a) Lin, T.-P.; Ke, I.-S.; Gabbaï, F. P. σ-Accepting Properties of a Chlorobismuthine Ligand. *Angew. Chem., Int. Ed.* **2012**, *51*, 4985−4988. (b) Jones, J. S.; Wade, C. R.; Gabbaï, F. P. Redox and Anion Exchange Chemistry of a Stibine−Nickel Complex: Writing the L, X, Z Ligand Alphabet with a Single Element. *Angew. Chem., Int. Ed.* **2014**, *53*, 8876−8879.

https://doi.org/10.1021/acs.organomet.3c00493
Organometallics 2024, 43, 634−652